

Robust power management capabilities of integrated energy systems in the smart distribution network including linear and non-linear loads

Original

Robust power management capabilities of integrated energy systems in the smart distribution network including linear and non-linear loads / Jin, Kai; Banizaman, Hamed; Samadi Gharehveran, Sina; Jokar, Mohammadreza; Mohammadi Amidi, Alireza; Yu, Jianyong; Oleiwi Shami, Hayder. - In: SCIENTIFIC REPORTS. - ISSN 2045-2322. - 15:(2025). [10.1038/s41598-025-89817-0]

Availability:

This version is available at: 11583/3007779 since: 2026-02-19T15:34:15Z

Publisher:

Nature

Published

DOI:10.1038/s41598-025-89817-0

Terms of use:

This article is made available under terms and conditions as specified in the corresponding bibliographic description in the repository

Publisher copyright

(Article begins on next page)



OPEN Robust power management capabilities of integrated energy systems in the smart distribution network including linear and non-linear loads

Kai Jin¹, Hamed Banizaman^{2✉}, Sina Samadi Gharehveran³, Mohammad Reza Jokar⁴, Alireza Mohammadi Amidi⁵, Jianyong Yu¹ & Hayder Olewi Shami⁶

This research presents the best power management of flexible-renewable integrated energy systems (FRIESs) with smart distribution networks (SDNs) by taking nonlinear load harmonic compensation into account. A deterministic model that optimizes for three distinct goals serves as the foundation for the proposed system. The goal is to minimize the combined impact of the network's operational costs, energy losses, and voltage harmonic distortion, taking into account their respective weights. In the FRIES framework, the goal function serves as a constraint on the operation of flexible and renewable sources, as well as the AC optimum harmonic power flow model. The suggested design is first formulated using nonlinear programming, and it is then approximated to a linear model in order to quickly arrive at the one and only optimum solution to the issue by different solvers. Furthermore, there is inherent uncertainty in the design of this work about the output power of renewable sources, load demand, energy consumption of mobile storage devices, and energy costs. Adaptive robust optimization has been applied to develop solutions that effectively address these uncertainties. Ultimately, the results show that, even with the aforementioned uncertainties, the SDN operation is resilient up to a maximum prediction error of 45%. Furthermore, if the distribution substation power factor is maintained at or above 0.9, the worst-case implemented design may enhance the network's energy losses, voltage profile, and harmonic status by 8.2%, 43.5%, and 51.2%, respectively, as compared to load flow studies.

Keywords Power management, Harmonic compensation, Flexible-renewable integrated energy system, Smart distribution network, Multi-objective operation, Adaptive robust optimization

List of symbols

Indices

h	Harmonic
i	FRIES
l	Auxiliary index corresponding to bus
m	Regular polygon planes
n	Bus
o	Operation hour
v	Segments in the piecewise linearization technique

Variables

Cost	Network operation cost (\$)
EL	Network energy losses (\$)

¹Sanya Research Institute, Hunan University of Science and Technology, Sanya 572000, China. ²Department of Electrical and Computer Engineering, Jahrom Branch, Islamic Azad University, Jahrom, Iran. ³Faculty of Electrical and Computer Engineering, Tabriz University, Tabriz, Iran. ⁴Department of Electronics and Telecommunication, Polytechnic University of Turin, Turin, Italy. ⁵Department of Electrical Engineering, Razi University of Kermanshah, Kermanshah, Iran. ⁶Al-Amarah University College, Maysan, Iraq. ✉email: ha.banizaman@iau.ac.ir

I_R, I_{EV}	Harmonic flow of renewable energy source (RES) and aggregation of electric vehicle (EVs) in terms of p.u.
I_C, I_V, I_L	Harmonic current of distribution substation, FRIES and distribution line (p.u.)
P_B, P_{LO}	Active power of battery and EV charger losses (p.u.)
P_{DR}	Active load response rate (DRP) power in p.u.
P_{EV}, Q_{EV}	Active and reactive power of EVs aggregation (p.u.)
P_L, Q_L	Active and reactive power of distribution line (p.u.)
P_S, Q_S	Active and reactive power of substation distribution (p.u.)
P_V, Q_V	Active and reactive power of FRIES (p.u.)
Q_R	Reactive power of RES (p.u.)
SHV	Total harmonic voltage (p.u.)
TVT	Total harmonic distortion (THD) voltage
$V, \Delta V$	Voltage range and voltage deviation (p.u.)
β	Voltage angle (radians)
κ, ω	Dual variable
τ_V	THD of voltage

Parameters

a, b	EVs charger loss coefficients
CR	EVs charging rate (p.u.)
G_L, B_L, Y_L	Distribution line conduction, suspension and admittance (p.u.)
\bar{I}	Bus and FRIES incidence matrix
\bar{I}_R, \bar{I}_{EV}	Maximum harmonic current of RES and aggregation of EVs (p.u.)
\bar{I}_S	Maximum harmonic current of distribution post (p.u.)
J	Bus and distribution line incidence matrix
n_m	Number of regular polygon planes
n_v	Quantity of segments in the piecewise linearization method
P_C, Q_C, I_C	Active and reactive power and harmonic current consumption (p.u.)
P_R	Active power of RES (p.u.)
\bar{S}_L, \bar{S}_S	Capacity (maximum apparent power) of distribution line and substation (p.u.)
\bar{S}_R, \bar{S}_{EV}	Capacity (maximum apparent power) of RES and aggregation of EVs (p.u.)
TCE	Consumption energy of EVs aggregation (p.u.)
\underline{V}, \bar{V}	Voltage range limits (p.u.)
γ	Cost of energy (\$/MWh)
ω	Consumer participation rates in DRP
$\omega_C, \omega_E, \omega_T$	Weighting coefficients

Motivation

The rise in concerns over the use of fossil fuels has resulted in a recent increase with the adoption of electric vehicles (EVs) and renewable energy technologies (RESs). However, the power system, particularly the distribution network, has a number of difficulties as a result of the connectivity of these resources, which ignores effective energy management¹. For example, adding more RESs to the network and injecting high active power might lead to overvoltage problems. Furthermore, the lack of energy management for EVs can lead them to perform charging operations during peak periods. This would eventually increase the number of EVs in the network and correspondingly result in severe voltage reduction and congestion in distribution lines, and escalation of network energy dissipation¹. However, encouraging the technical and economic indicators in distribution systems would be a good start via proper energy management of the aforementioned resources². The distribution system operator (DSO) is eager to generate active electricity by using the maximum production of RESs as they also have low operational expenses. Furthermore, under the aforementioned circumstances, energy storage systems (ESS)³ or demand response programs (DRP) are used to enhance the network's technical and economic metrics⁴. In fact, DRP and ESS are able to store the surplus generation of RESs in low-consumption periods of the grid and inject the stored power to the grid in peak-consumption hours⁴. Therefore, it is estimated that a significant number of environmentally friendly resources, such as RESs, ESSs, and DRP, contribute to the distribution network operation. A distribution network equipped with the mentioned resources can have the desired economic and technical status if an energy management system is suitably designed and operated⁵. The first step is then to establish proper coordination between the various energy entities and their coordination with the DSO⁵. An appropriate solution is to use aggregating platforms such as integrated energy systems (IESs) for the coordination of the grid resources. According to⁶, the coordination of the mentioned resources in the form of IES can have more favorable economic and technical results than the individual management of each resource in the network. Therefore, it is anticipated that with the optimal operation of distribution networks when IESs are present, the desired condition can be achieved for various system indicators such as operation, security, and dependability.

Literature review

Numerous studies have been done on how IESs function in distribution networks. In⁷, authors modeled a coordinated optimum power flow in a distribution system and IES (such as virtual power plant (VPP)) by employing a decentralized method coupled with the bender's decomposition and multi-parametric quadratic programming. The quadratic exchange functions are constructed in feasible sub-problems, quickening the convergence process. On the other side, feasible cut sets are built using benders decomposition in infeasible sub-problems. In addition, an efficient relaxation method is implemented for addressing the problem of degeneracy.

A predefined feasible area is determined based on the characteristic of each IES in order to eliminate the extra feasible cut sets. The authors of⁸ presented a system that maximizes the IES power supply for a number of markets, including reserve and energy. In addition, various system components such as local network services, inertia, quick frequency response, and upstream reactive power are handled with the goal of maximizing profits. To get assured that the problem is tractable, which also requires to be operated considering the limitations of the local network and addresses the uncertainties of electricity price, RES outputs, and load demand, the proposed scheme is divided into three correlated optimization problems. More specifically, two receding horizon optimization approaches for near-real-time dispatch are introduced. These include a detailed quadratic cone relaxation for power flows and a robust optimization method⁹ that considers multiple scenarios for day-ahead resource planning, incorporating linearized power flow equations¹⁰. elaborates on the capabilities of photovoltaic pumped storage (HPP) in energy markets and proposes a two-stage strategy for managing congestion for IESs like VPP. Using a genetic algorithm, the Independent System Operator (ISO) oversees congestion management in the initial stage with the goal of minimizing it. In the next step, a multi-objective optimization model that considers ecological and navigational issues for light and water reduction is used to regulate the power at the IES. In¹¹, a bi-level optimization issue is proposed by modeling a wide variety of pricing for active and reactive power for the coordinated management of an active distribution network (ADN) with various IESs (VPPs). In the upper-level issue, the overall network operating cost with respect to system security and player interaction (VPPs, ADN, and market operator) is reduced. The lower-level sub-problem then takes into account many flexible sources in order to optimize the profitability of each VPP. An ideal management strategy for an IES engaging in both day-ahead and real-time energy markets was outlined in Ref¹². Because of this, the combination of distributed energy resources (DERs) might maximize revenues while managing real-time swings resulting from resource unpredictability. Some of the DERs bidding strategies of the implemented design include VPP, DPR aggregation, electric vehicles, and micro-grid. The VPP is responsible for the determination of internal prices, which are applied to the DERs aggregation using real-time feedbacks to the daily schedules. The VPP also updates suggested parameters of pricing function, and finally, the DERA sets its reserve energy. In another research¹³, the authors addressed the challenge of developing an optimal bidding strategy for the IES participation in three electricity markets, as day-ahead market, real-time market, and spinning reserve market. The IES is scheduled as a multistage risk-constrained stochastic problem. In this problem, uncertainties root in the electricity prices, renewable generation, loads, and the need for reserve services.

A two-layer energy management system (EMS) that takes use of IESs like VPPs is introduced in the AND. These units participate effectively in both the reserve and day-ahead energy markets. The VPPs optimize market profits in the first layer while adhering to variable resource limits, RESs, and resource-VPP operator cooperation. In the second layer, the distribution system operator and the VPP operator coordinate to control the ADN based on the network energy loss summation and voltage deviation function minimization, taking into account the boundaries of linear AC optimum power flow. In¹⁴, a novel design is presorted for the optimal bidding strategies of the technical VPP in various markets, aiming to promote the role of DERs in electricity markets. The proposed framework postulates that the distribution of technical VPP is carried out across a multi-energy network, comprising district heat and electricity networks. In their publication, the authors of reference¹⁵ introduced a novel analytical framework aimed at assessing the viability of leveraging the VPP to generate advantages for both the demand side and the plant. The model firstly explores the potentials of energy-saving of the VPP consisting of photovoltaics (PV) and ESS. Secondly, The VPP's economic indicators were assessed utilizing a comprehensive life cycle cost analysis and payback period methodology. Afterward, a cooperative game was suggested for exploring the participation potential by taking into account the profit inequality of the plant and demand side. In a related study¹⁶, the researchers created an ideal network partition model to reduce the power injection fluctuation at the common coupling point (CPP) and the voltage variances within IESs. Using a unique convex formulation of network reconfiguration technique, this approach ensures that the same IES components will remain connected and that the IES's performance will continue to improve. In¹⁷, a real-time algorithmic framework is created for the purpose of aggregating ADN resources and providing regulating services upon transmission system operator (TSO) request¹⁸. A theoretical framework based on the online primal-dual method has been constructed in this research to successfully accomplish the goal of IESs at the distribution system. This approach is appropriate for optimization problems¹⁹ that involve time-dependent variables and performing linearization of the nonlinear AC power-flow equations. In²⁰, the effects of participating ESSs on an IES model and correspondingly utilizing it to perform generation system adequacy studies is investigated. A two-stage linearization method is suggested to develop the general IES model with the features of aggregation and size of various distributed generators (DG), ESSs and loads along with ADN information such as constraints and topology. Reference²¹ introduced an energy management strategy for an Integrated Energy System (IES) that addresses the balance of electricity, heat, and hydrogen supply and demand, along with uncertainties in demand. The proposed approach is structured into three phases: a day-ahead scheduling phase, a model predictive control (MPC) based intraday rolling dispatch phase, and an intraday real-time adjustment phase. This framework is designed to engage in both electricity and hydrogen markets. Reference²² outlines the energy management strategy for a smart distribution network that incorporates hydrogen storage and renewable energy sources. The goal is to evaluate various aspects such as economic efficiency, operational performance, flexibility, and reliability from the perspective of the distribution system operator. The objective function aims to reduce operational costs, enhance reliability, minimize energy losses, and improve network flexibility. The approach is subject to constraints including AC optimal power flow equations, reliability requirements, and the integrated system model. In reference²³, a cooperative game model for an integrated energy system across industrial, commercial, and residential zones is developed using Nash bargaining theory. This model focuses on the collaborative management of multiple energy parks, which have varying operational characteristics, to facilitate energy sharing and joint dispatching strategies. Reference²⁴ introduces an optimal scheduling framework for an active distribution network (ADN) incorporating renewable

energy sources (RESs) alongside flexible resources (FSs), including non-renewable energy sources (NRESs) and electric vehicle (EV) charging stations, utilizing adaptive robust optimization (ARO)²⁵. This approach involves a deterministic programming model with a focus on two primary objectives for optimization. Reference²⁶ outlines a combined stochastic and robust approach for coordinated power management (CPMS) aimed at enhancing the flexibility, reliability, and security metrics of microgrids (MGs). This strategy addresses the integration of electric vehicles (EVs), energy storage systems (ESS)²⁷, distributed generation (DG), and demand response programs (DRP).

In²⁸, optimal power flow (OPF) for microgrids is discussed. Its goal is to maintain voltage control while minimizing power distribution losses or the cost of electricity supplied by DGs that are obtained from the substation. Disparate loads in each phase and non-equidistant conductor spacings on the distribution lines cause the microgrid to become unbalanced. The OPF problem in question is nonconvex, similar to OPF formulations for balanced systems. However, a convex problem with polynomial-time complexity is derived using a semidefinite programming (SDP) relaxation technique. To mitigate three-phase imbalance and minimize active power losses in distribution networks, a hybrid optimization method employing Y-connected and Δ -connected static reactive power compensation devices is introduced. Instead of concentrating on a single feeder or particular location, the idea is to optimize the performance of every device to reduce the imbalance of the entire distribution network. Before developing a framework for modeling energy technologies with intertemporal characteristics in the context of active network management, Reference³⁰ looks at the general formulation of dynamic OPF. A thorough optimization model for a flexible distribution network that guarantees both system security and financial efficiency is presented in Reference³¹. In order to minimize loss and voltage deviation, the OPF model for a flexible distribution network—which incorporates numerous active management mechanisms—is developed. Table 1 provides a summary of the literature.

Research gaps

The following are the primary knowledge gaps concerning the functioning of network-based IESs, as identified by the background research and displayed in Table 1:

- In most management researches such as^{7,10–17,20–23,28–31} only the active power management of IESs has been discussed. However, in an IES, both active and reactive power may be concurrently controlled by RESs and ESS. For example, sources based on synchronous generators may freely regulate two different forms of electricity at the same time. With the right electronic power converter (bidirectional converter with IGBT or MOSFET bridge), RESs and ESSs (like batteries) may also regulate these two forms of powers; nevertheless, they will need to pay for the upgrade of the converter structure. Therefore, an IES can simultaneously control and manage its active and reactive power at the connection point to the network. Although the management of active power alone has a positive effect on the conditions of the network's technical indicators, the impact of reactive power on some other indicators such as voltage profile and safety is greater than active power²⁶. Reactive power control devices were adopted for voltage regulation purposes²⁶. Therefore, reactive power management of IESs, in addition to its management of active power, can effectively promote the financial and technical outcomes of the distribution system. However, this issue has been extensively examined in recent studies^{8,11}.

Ref.	IES power management		Harmonic compensation with IES	EVs capability as flexibility sources	Uncertainty model
	Active	Reactive			
7	Yes	No	No	No	Stochastic
8	Yes	Yes	No	No	Stochastic-robust
10	Yes	No	No	No	Stochastic
11	Yes	Yes	No	No	Stochastic
12	Yes	No	No	Yes	Stochastic
13	Yes	No	No	No	Stochastic
14–17,20	Yes	No	No	No	Stochastic
21	Yes	No	No	No	Stochastic
22	Yes	No	No	No	Stochastic
23	Yes	No	No	No	Stochastic
24	Yes	Yes	No	No	ARO
26	Yes	Yes	No	No	Stochastic-robust
26	No	No	No	No	Stochastic
29	No	No	No	No	Stochastic
30	No	No	No	Yes	Stochastic
31	No	No	No	No	Robust
Proposed scheme	Yes	Yes	Yes	Yes	ARO

Table 1. The categorization of current research studies. ARO adaptive robust optimization.

- Some renewable energy sources (RESs), including wind turbines (WT) and photovoltaic (PV) systems, are integrated into the electricity grid through electronic power converters. For other ESSs, like batteries, this also holds true. If these resources employ a bidirectional electronic converter with an IGBT or MOSFET bridge, they would be able to adjust their harmonic current. Therefore, they might be useful in compensating for the harmonics of nonlinear loads. This is also true for IESSs, as they include RESs and ESSs. Nonetheless, IESSs' potential has received scant study concerning the harmonic compensation of nonlinear loads in recent researches.
- The integration of RESs within an energy system has been found to have a negative impact on the system's adaptability in response to uncertainties in their active production capacity. To compensate for this, it is recommended to adopt flexible tools and equipment such as non-renewable resources, DRP, ESS, and EVs alongside RESs is generally recommended. DRPs, batteries, and EVs are known as a desirable source of flexibility due to their constant power provision in power variations^{5,6}. But in fewer studies such as¹², EVs have been considered a source of flexibility. Note that DRPs and EVs are used by many energy customers, which can be considered for ancillary services such as improving network flexibility by providing an incentive program. However, the use of non-renewable resources and static storage facilities requires significant construction costs. Hence DRPs and EVs are more achievable than other types of resources and ESSs.
- Operation of network-connected IESSs is accompanied by various uncertainties such as load demand, RESs output power, market price, EVs. Also, the execution time interval in operational problems is usually less than one hour^{5,6}. Therefore, high convergence speed or low computing time is crucial for this kind of problems. To achieve these merits, the use of uncertainty modeling methods with the least number of scenarios is appropriate. Therefore, robust modeling with only one scenario will be appropriate to obtain this goal. However, this has been the case in fewer studies, and most studies^{7,10-17,20-23,28-30} adopted stochastic programming to model uncertain quantities. Stochastic programming includes a so many scenarios that reduce the speed of convergence. In addition, note that robust programming is performed in the worst-case scenario because of the uncertainties. Thus, it is capable of achieving an optimal solution that is robust against prediction errors arising from uncertainties³².

Contributions

To effectively address the aforementioned study gaps, the SDN's optimal operation with FRIESSs is formulated by taking into account the harmonic compensation of nonlinear network loads by FRIESSs (Fig. 1). The design's deterministic model is expressed through a three-objective optimization approach utilizing the sum of weighted functions methodology. Minimizing the SDN's operating expenses, energy losses in the grid, and voltage total harmonic distortion (THD) is the main goal of the target functions. The above described issue is also addressed by the AC harmonic optimum power flow (AC-HOPF) framework, which incorporates flexibility in the form of FRIESS and the use of RESs into the model. In this scheme, flexibility resources (FSs) include DRP and parking lot for EVs. The reason for choosing these sources is as follows: (1) The time constant of DRP and EV batteries in power change is very low. Therefore, they can more quickly correct RESs power fluctuations than their predicted data and improve system flexibility, (2) In the future, these environmentally friendly FSs are expected to be more accessible than other FSs such as non-renewable energy sources and ESSs because utilization of other FSs requires construction cost. But DRPs and EVs are generally distributed in the network and can be used as FSs by appropriate incentive programs. The problem is structured as nonlinear programming (NLP). But this scheme is known as an operational problem in the power system. The time interval for solving these problems is less than one hour. Therefore, the convergence speed is of particular importance in these problems¹¹. Using an

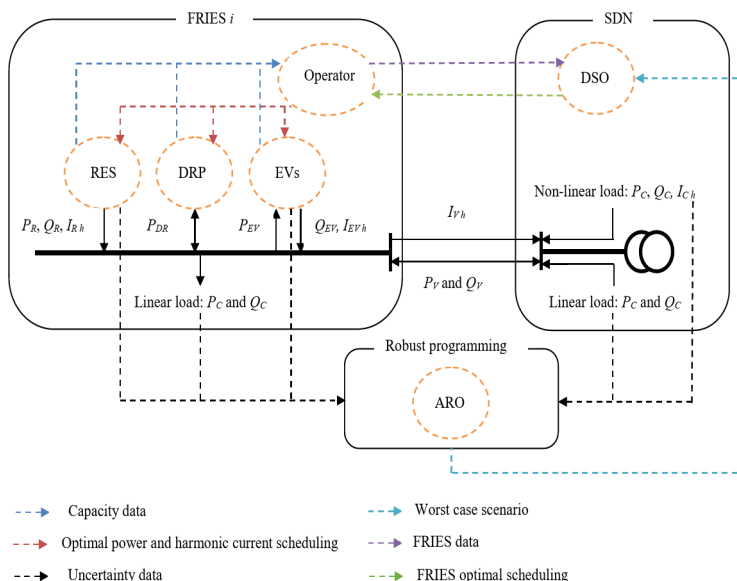


Fig. 1. Framework of FRIESSs operation in SDN.

appropriate linear approximation model (LAM) that has less errors than the base model of the recommended design is a very efficient way to do this. Consequently, a linearized model for power distribution equations as well as a circular plane pertaining to the capacity restrictions of different network components are provided using the first-order Taylor series approach and the traditional piecewise linearization methodology. In the shape of a regular polygon, it is comparable to a plane. Additionally, the LAM makes use of linear correlations that are comparable to the nonlinear model of harmonic indices like THD. Furthermore, there is uncertainty in this design about elements like energy price, load demand, RES power, and the combined energy consumption of the EVs. Adaptive robust optimization (ARO) is used in this study to extract a solution that is robust against the prediction error of the uncertainties. The computational time of the proposed structure based on robust optimization will be much less than that of stochastic and probabilistic modeling since the current technique just needs a scenario. Furthermore, the resultant outcome with this strategy is identical to the worst case. Robust optimization, therefore, offers a solution that is immune to uncertainty. This leads to the evaluation of the robust performance of FRIES in improving operational indicators and power quality (harmonic). In the end, the novelties of the paper are provided below.

- Simultaneous management of active and reactive power of the SDN with FRIES to enhance the economic and operation conditions of the network,
- Harmonic compensation of nonlinear loads in SDN by FRIESs to improve the power quality of network,
- Use of more accessible flexibility resources such as DRPs and EVs alongside RESs in the form of FRIES, and,
- Extract the robust abilities of FRIESs to boost the technical and economic indicators of the SDN against the forecast error of load uncertainties, RESs, EVs, and market prices.

Paper organization

The structure of the document is outlined in the following sections: The second section presents the linear approximation formulation and nonlinear modeling for the SDN operation in the presence of FRIESs. Section 3 then goes into the modeling of ARO uncertainties for the suggested approach. Findings are detailed in Sect. 4, while Sect. 5 contains the closing thoughts and phrases.

Deterministic modeling of scheme Non-linear formulation

When FRIES is present, SDN power management is developed and nonlinear load harmonic correction is used. The plan looks for the lowest possible THD bus voltage, energy losses, and overall weighted operating cost of SDN. Additionally, the operational model of FSs and RESs in the form of FRIES is applied, together with the AC-HOPF limitations. As a result, the following will be the model for the suggested design:

(A) *objective function*: Eq. (1) defines the goal of minimizing the overall weighted cost of the SDN (Part I), the energy losses (EL) of the network (Part II)³³, and the total THD is the bus voltage (TVT - Part III)³⁴. The purchase of SDN energy sourced from the upstream network is referred to as the network's operating cost. This is accomplished by multiplying the energy price by the distribution substation's hourly throughput. The distinction between the SDN's energy generation and consumption is known as the EL network. Additionally, TVT is equivalent to the total THD voltage across all buses throughout all operating hours. Furthermore, Eq. (1) employs the weighted sum of functions in multi-objective optimization. The summation of weighting coefficients ω_C , ω_E and ω_T must always be equation to 1³⁵. In this method, Cost, EL, and TVT functions depend on weighting coefficients, shown as 3D plot for the Pareto front of the suggested scheme³³. In the following, the fuzzy decision method selects the compromise approach that balances the specified functions³³. Fuzzy method calculates the linear membership function for Cost, EL, and TVT functions for a certain value ω_C , ω_E and ω_T . Suppose the objective function's value is greater (or smaller) than its maximum function value (Cost^{\max} , EL^{\max} and TVT^{\max}). In that case, the linear membership function value for that objective function is zero (1). Otherwise, the value of the linear membership function equals dividing the discrepancy between the objective function and its maximum and the range of changes of this objective function. The minimum (Cost^{\min} , EL^{\min} and TVT^{\min}) and the highest values of each objective function can also be derived from solving three problems, (1) $\omega_C=1$, (2) $\omega_E=1$, and (3) $\omega_T=1$. The varying range of each objective function is the difference between its minimum and maximum values. In the next step, for a certain value ω_C , ω_E and ω_T the minimum value of the linear membership function is extracted, which is represented by π in this section. The compromise solution is equal to the point with the highest value π on the Pareto front³³.

$$\min \frac{\omega_C}{\text{Cost}^{\max} - \text{Cost}^{\min}} \cdot \overbrace{\sum_o \gamma_o P_{S n=s,o}}^{\text{Cost}} + \frac{\omega_E}{\text{EL}^{\max} - \text{EL}^{\min}} \cdot \overbrace{\sum_{n,o} \left(P_{S n,o} + \sum_i (I_{i,n} P_{V i,o}) - P_{C n,o} \right)}^{\text{EL}} + \frac{\omega_T}{\text{TVT}^{\max} - \text{TVT}^{\min}} \cdot \overbrace{\sum_{n,o} \tau_{V n,o}}^{\text{TVT}} \quad (1)$$

(B) *AC-HOPF constraints in SDN*: The constraints of this section are presented in Eq. (2) to (13)^{34,36}. Thus, constraints (2)-(9) represent the harmonic power distribution equations (HPF), and the operating and harmonic constraints are shown in constraints (10)-(13). It is worth noting that there are two models for the HPF³⁶. The first model assumes that the main frequency components ($h=1$), voltage, and current are the main factors of active and reactive power³⁶. Therefore, the apparent power can be determined by multiplying the voltage and the current conjugate at $h=1$. Following this, the HPF model will include the AC power flow model (AC-PF), constraints (2)-(6), and the harmonic current distribution model at $h \neq 1$, (7)-(8). In the second HPF model, it is assumed that all frequency components ($h=1, 2, \dots$), voltage, and current are the main factors for the emergence of power in the element. Therefore, the apparent power in this model is the sum of multiplication of voltage and current conjugate in all frequency components. The results of the two models are unique^{34,36}, but the formulation of the second model of the HPF is more complex than the first model³⁴. As a result, the first HPF model is employed, which is based on constraints (2)-(8). AC-PF refers to the formulation of active and reactive power balancing in SDN buses, active and reactive power flow via the distribution line, and the reference bus voltage. The harmonic current distribution at h is also represented by Eqs. (7) and (8), which indicate the current balance at each bus and the current going via the distribution line, respectively. The THD voltage for SDN buses at various operation hours is computed in Eq. (9)³⁴. Constraints (10)–(13) include SDN operational and harmonic limitations^{2,34}. Operating limitations include the maximum voltage range of the bus in the major harmonic component, (12) per $h=1$, and the maximum capacity (apparent power) of the distribution line and substation, (10) and (11). The harmonic constraint also includes the limit of the harmonic voltage range, (12) per $h \neq 1$, and the boundary of the harmonic current passing through the distribution substation, (13)³⁴. As another point, in the constraints of this section, the assumption is made that the SDN is linked to the upstream network by means of a distribution substation that is situated on the reference bus. So, the values of P_s , Q_s , and I_s variables are zero for all buses except the reference bus. Also, the lower limit of the voltage range at h is equal to zero, and the upper limit according to IEEE519 standard is equal to 3% or 0.03 per unit. Lastly, the variables κ and ω denote the dual variables associated with equality and inequality constraints, respectively. Active and reactive power changes based on model (2)-(13) have an effect on the main frequency components of voltage and current, and the harmonic components of voltage and current are not dependent on active and reactive power.

$$P_{S n,o} + \sum_i I_{i,n} P_{V i,o} - \sum_l J_{l,n} P_{L n,l,o} = P_{C n,o} : \kappa_{P n,o} \quad \forall n, o \tag{2}$$

$$Q_{S n,o} + \sum_i I_{i,n} Q_{V i,o} - \sum_l J_{l,n} Q_{L n,l,o} = Q_{C n,o} : \kappa_{Q n,o} \quad \forall n, o \tag{3}$$

$$P_{L n,l,o} = G_{L n,l,h=1} (V_{n,o,h=1})^2 - V_{n,o,h=1} V_{l,o,h=1} \left\{ \begin{array}{l} G_{L n,l,h=1} \cos(\beta_{n,o} - \beta_{l,o}) \\ + B_{L n,l,h=1} \sin(\beta_{n,o} - \beta_{l,o}) \end{array} \right\} : \kappa_{P L n,l,o} \quad \forall n, l, o \tag{4}$$

$$Q_{L n,l,o} = -B_{L n,l,h=1} (V_{n,o,h=1})^2 + V_{n,o,h=1} V_{l,o,h=1} \left\{ \begin{array}{l} B_{L n,l,h=1} \cos(\beta_{n,o} - \beta_{l,o}) - \\ G_{L n,l,h=1} \sin(\beta_{n,o} - \beta_{l,o}) \end{array} \right\} : \kappa_{Q L n,l,o} \quad \forall n, l, o \tag{5}$$

$$\beta_{n,o} = 0 : \kappa_{\beta n,o} \quad \forall n = s, o \tag{6}$$

$$I_{S n,o,h} + \sum_i I_{i,n} I_{V i,o,h} - \sum_l J_{l,n} I_{L n,l,o,h} = I_{C n,o,h} : \kappa_{I n,o,h} \quad \forall n, o, h \neq 1 \tag{7}$$

$$I_{L n,l,o,h} = Y_{L n,l,h} (V_{n,o,h} - V_{l,o,h}) : \kappa_{I L n,l,o,h} \quad \forall n, l, o, h \neq 1 \tag{8}$$

$$\tau_{V n,o} = \frac{\sqrt{\sum_{h \neq 1} (V_{n,o,h})^2}}{V_{n,o,h=1}} : \kappa_{T n,o} \quad \forall n, o \tag{9}$$

$$(P_{L n,l,o})^2 + (Q_{L n,l,o})^2 \leq (\bar{S}_{L n,l})^2 : \bar{\omega}_{S L n,l,o} \quad \forall n, l, o \tag{10}$$

$$(P_{S n,o})^2 + (Q_{S n,o})^2 \leq (\bar{S}_{S n})^2 : \bar{\omega}_{S S n,o} \quad \forall n = s, o \tag{11}$$

$$\underline{V}_h \leq V_{n,o,h} \leq \bar{V}_h : \underline{\omega}_{V n,o,h}, \bar{\omega}_{V n,o,h} \quad \forall n, o, h \tag{12}$$

$$-\bar{I}_{S n,h} \leq I_{S n,o,h} \leq \bar{I}_{S n,h} : \underline{\omega}_{I S n,o,h}, \bar{\omega}_{I S n,o,h} \quad \forall n = s, o, h \neq 1 \tag{13}$$

C) *FRIES constraints*: Constraints on the performance of RESs and flexibility in the form of FRIES are presented in Eqs. (14)-(15). Therefore, the active and reactive power balances are modeled in Eqs. (14) and (15), respectively, and the current balance in the harmonic frequency components ($h \neq 1$) is formulated in Eq. (16). The following provides the mathematical modeling of the energy sources. In (17) and (18), the RESs formulations are presented. Equations (17) and (18) indicate the limit of capacity (apparent power) / controllable harmonic current of the electronic converter between the RES and the network^{2,5}. The DRP model based on encouragement (as an FS) is formulated in clauses (19) and (20). In this model, based on the price signal in the first part of the Eq. (1), consumers transfer a portion of their energy demand during peak period (higher energy price) to low peak period (lower energy price). This aligns with the goal of reducing the operating cost of SDN or Part I of Eq. (1). Therefore, constraint (19) considers a range of active power of consumers in DRP, assuming that their participation rate in the DRP is equal to ω . Equation (20) also ensures that FRIES provides all energy demand in low load period. Finally, the EV model of parking lot operation is presented in constraints (21)-(26). Equation (21) shows the active power balance between EV batteries and EV power from a network perspective. Active power loss of chargers is calculated in Eq. (22). In constraints (23), the energy consumption model of all electric vehicles connected to a bus is expressed. In this article, it was assumed that EVs only use their battery charging mode. Therefore, their total charging power in the horizon of operation should be equal to the energy they need for traveling in the future. Equation (24) also limits the charge rate of accumulation of the EV batteries. The limit of apparent power/controllable harmonic current of the aggregators of EV chargers is formulated in Eqs. (25) and (26). It is noteworthy that chargers are used to connect the batteries to the network in EVs. According to³², if a bidirectional DC-AC converter is used in the charger, the active and reactive power and the harmonic current of the EVs can be controlled simultaneously. The flexible loads include DRP and EVs in this paper. DRP control only active power, and it does not perform harmonic compensation. EVs can compensate the harmonic current. According to³², EVs include a charger, and charger includes a power electronic system. Charge can be controlled harmonic current based on³².

$$P_{V i,o} = P_{R i,o} + P_{DR i,o} - P_{EV i,o} - P_{C i,o} : \kappa_{PV i,o} \quad \forall i,o \tag{14}$$

$$Q_{V i,o} = Q_{R i,o} - Q_{EV i,o} - Q_{C i,o} : \kappa_{QV i,o} \quad \forall i,o \tag{15}$$

$$I_{V i,o,h} = I_{R i,o,h} + I_{EV i,o,h} - I_{C i,o,h} : \kappa_{IV i,o,h} \quad \forall i,o,h \neq 1 \tag{16}$$

$$(P_{R i,o})^2 + (Q_{R i,o})^2 \leq (\bar{S}_{R i})^2 : \bar{\omega}_{SR i,o} \quad \forall i,o \tag{17}$$

$$-\bar{I}_{R i,h} \leq I_{R i,o,h} \leq \bar{I}_{R i,h} : \underline{\omega}_{IR i,o,h}, \bar{\omega}_{IR i,o,h} \quad \forall i,o,h \neq 1 \tag{18}$$

$$-\varpi_i P_{C i,o} \leq P_{DR i,o} \leq \varpi_i P_{C i,o} : \underline{\omega}_{DR i,o}, \bar{\omega}_{DR i,o} \quad \forall i,o \tag{19}$$

$$\sum_o P_{DR i,o} = 0 : \kappa_{DR i} \quad \forall i \tag{20}$$

$$P_{EV i,o} = P_{B i,o} + P_{LO i,o} : \kappa_{PE i,o} \quad \forall i,o \tag{21}$$

$$P_{LO i,o} = a_i |P_{EV i,o}| + b_i |Q_{EV i,o}| : \kappa_{PLO i,o} \quad \forall i,o \tag{22}$$

$$\sum_o P_{B i,o} = TCE_i : \kappa_{PB i} \quad \forall i \tag{23}$$

$$0 \leq P_{B i,o} \leq CR_{i,o} : \bar{\omega}_{PB i,o} \quad \forall i,o \tag{24}$$

$$(P_{EV i,o})^2 + (Q_{EV i,o})^2 \leq (\bar{S}_{EV i,o})^2 : \bar{\omega}_{SE i,o} \quad \forall i,o \tag{25}$$

$$-\bar{I}_{EV i,o,h} \leq I_{EV i,o,h} \leq \bar{I}_{EV i,o,h} : \underline{\omega}_{IE i,o,h}, \bar{\omega}_{IE i,o,h} \quad \forall i,o,h \neq 1 \tag{26}$$

Linear approximation model

The issue mentioned previously includes a non-convex nonlinear model arising from nonlinear limitations (4), (5), (9)-(11), (17), (22) and (25), and non-convex constraints (4) and (5). Common commercial solvers often find a local optimum solution since the issue is non-convex^{5,34}. Therefore, these solvers cannot extract a single solution^{2,5}. Their lengthy computation times are due to the fact that they also rely on numerical computations that are dependent on repetition. But among the difficulties in operating a power system are formulations (1) through (26) where a fast convergence speed is particularly crucial. Therefore, the linear approximation model is employed for the suggested design in order to quickly arrive at a single ideal solution. Also, the main objective of paper according to Sect. 1 is robust modelling of the proposed scheme. Robust optimization needs to the dual model of the proposed formulation. Dual model needs to convex and linear formulation. Therefore, this paper employs a linear approximation model. The specifics of this modeling are outlined below. Based on³⁴, the voltage angle difference between the two buses at the start and end of a distribution line is under 6 degrees or 0.105 radians. Thus, the expressions $\cos(\beta_{n,o} - \beta_{l,o})$ and $\sin(\beta_{n,o} - \beta_{l,o})$ are approximated to 1 and $(\beta_{n,o} - \beta_{l,o})$ based on the Taylor series, respectively. In addition, the voltage amplitude (V) variable based on the linear piecewise linearization technique is represented as $V_{h=1} + \sum_v \Delta V_v$ in which ΔV is the

voltage deviation³⁴. Subsequently, the expressions V^2 and $V_n V_l$ are formulated $(\underline{V}_{h=1})^2 + \sum_{\nu} slop_{\nu} \Delta V_{\nu}$ and $(\underline{V}_{h=1})^2 + \sum \Delta V_{n,\nu} + \Delta V_{l,\nu}$, respectively. Here, the slope indicates the linear slope. Now, by neglecting the values ΔV^2 , $\Delta V_n \Delta V_l$ and $\Delta V \times (\beta_n - \beta_l)$ given their minimal values, the linear approximation for Eqs. (4) and (5) can be expressed as follows:

$$P_{L\ n,l,o} = G_{L\ n,l,h=1} \left(\sum_{\nu} (slop_{\nu} - \underline{V}_{h=1}) \Delta V_{n,o,\nu} - \underline{V}_{h=1} \Delta V_{l,o,\nu} \right) \tag{27}$$

$$-(\underline{V}_{h=1})^2 B_{L\ n,l,h=1} (\beta_{n,o} - \beta_{l,o}) : \kappa'_{P_{L\ n,l,o}} \quad \forall n, l, o$$

$$Q_{L\ n,l,o} = -B_{L\ n,l,h=1} \left(\sum_{\nu} (slop_{\nu} - \underline{V}_{h=1}) \Delta V_{n,o,\nu} - \underline{V}_{h=1} \Delta V_{l,o,\nu} \right) \tag{28}$$

$$-(\underline{V}_{h=1})^2 G_{L\ n,l,h=1} (\beta_{n,o} - \beta_{l,o}) : \kappa'_{Q_{L\ n,l,o}} \quad \forall n, l, o$$

In proportion to the use of the piecewise linearization method for the voltage range, in Eq. (12), the voltage deviation limit as in Eq. (29) will replace the voltage range limit at $h=1$. Under these conditions, the voltage amplitude constraint in the harmonic frequency components ($h \neq 1$) is separated as constraint (30) from constraint (12).

$$0 \leq \Delta V_{n,o,\nu} \leq \frac{\bar{V}_{h=1} - \underline{V}_{h=1}}{n_{\nu}} : \bar{\omega}_{\Delta V\ n,o,\nu} \quad \forall n, o, \nu \tag{29}$$

$$\underline{V}_h \leq V_{n,o,h} \leq \bar{V}_h : \underline{\omega}_{V\ n,o,h}, \bar{\omega}_{V\ n,o,h} \quad \forall n, o, h \neq 1 \tag{30}$$

Constraints (10)-(11), (17), and (25) represent a circular plane with origin point and radius S in the coordinates of PQ, i.e. $P^2 + Q^2 \leq S^2$. To express a linear model for them, a circular plane is approximated by representing it as a regular polygon. So that if the number of planes is high, the computational error between the two pages will be very low. According to, the line equation is equal for one plane $P \times \cos(m \times \Delta\phi) + Q \times \sin(m \times \Delta\phi) = S$, where m represents the plane and $\Delta\phi$ denotes the angle deviation. $\Delta\phi$ is $360/n_m$, where n_m represents the total number of planes in a regular polygon. Now, the plane of each side is in the form, which repeats this equation for all sides ($m = 1, 2, \dots, n_m$) to extract a plane in the form of a regular polygon. Accordingly, the linearized model of constraints (10)-(11), (17), and (25) is as follows:

$$P_{L\ n,l,o} \cos(m \times \Delta\phi) + Q_{L\ n,l,o} \sin(m \times \Delta\phi) \leq \bar{S}_{L\ n,l} : \bar{\omega}'_{S_{L\ n,l,o,m}} \quad \forall n, l, o, m \tag{31}$$

$$P_{S\ n,o} \cos(m \times \Delta\phi) + Q_{S\ n,o} \sin(m \times \Delta\phi) \leq \bar{S}_{S\ n} : \bar{\omega}'_{S_{S\ n,o,m}} \quad \forall n = s, o, m \tag{32}$$

$$P_{R\ i,o} \cos(m \times \Delta\phi) + Q_{R\ i,o} \sin(m \times \Delta\phi) \leq \bar{S}_{R\ i} : \bar{\omega}'_{S_{R\ i,o,m}} \quad \forall i, o, m \tag{33}$$

$$P_{EV\ i,o} \cos(m \times \Delta\phi) + Q_{EV\ i,o} \sin(m \times \Delta\phi) \leq \bar{S}_{EV\ i,o} : \bar{\omega}'_{S_{EV\ i,o,m}} \quad \forall i, o, m \tag{34}$$

The active battery power of EVs (P_B) has a positive value based on the constraint (24), so the P_{EV} variable will always be positive. Hence the term $|P_{EV}|$ in Eq. (22) is equal to P_{EV} . The distribution network also has a significant resistance-admittance load, so reactive power devices such as EV parking lots are operated in capacitive mode. Hence, the term $|Q_{EV}|$ will be equal to $-Q_{EV}$. In this case, constraint (22) will be rewritten as Eq. (35), provided that the Q_{EV} constraint will be the same as constraint (36).

$$P_{LO\ i,o} = a_i P_{EV\ i,o} - b_i Q_{EV\ i,o} : \kappa'_{P_{LO\ i,o}} \quad \forall i, o \tag{35}$$

$$-\bar{S}_{EV\ i,o} \leq Q_{EV\ i,o} \leq 0 : \underline{\omega}_{Q_{EV\ i,o}} \quad \forall i, o \tag{36}$$

Constraint (9), which calculates the voltage THD, also has a nonlinear relation. Since this relation is used only in the objective function, it is possible to use an equivalent relation with TVT in the third part of Eq. (1), so that an optimal point is extracted in two cases. In TVT, the goal is to minimize the THD voltage, following which the voltage amplitude in the harmonic frequency component ($h \neq 1$) tends toward zero. Accordingly, the term

$\sum_{n,o,h \neq 1} V_{n,o,h}$ can replace the TVT relation in the third part of the Eq. (1). Because this expression directly minimizes the voltage range at $h \neq 1$. In these circumstances, Eq. (9) can be removed. Ultimately, the linear approximation approach for the suggested design is expressed as:

$$\begin{aligned} \min \quad & \omega_C \cdot \sum_o \gamma_o P_{S_{n=s,o}} \\ & + \omega_E \cdot \sum_{n,o} \left(P_{S_{n,o}} + \sum_i (I_{i,n} P_{V_{i,o}}) - P_{C_{n,o}} \right) \\ & + \omega_T \cdot \sum_{n,o,h \neq 1} V_{n,o,h} \end{aligned} \tag{37}$$

Subject to:

$$\text{Constraints(2), (3), (6) – (8), (13) – (16), (18) – (21), (23), (24), (26) – (36)} \tag{38}$$

In the linearization technique described in this section, based on³⁴, the calculation error for active and reactive power is approximately 1.2–1.5%. The calculation error for voltage is less than 0.5%. As another point, in this article, only the voltage magnitude variable was converted to other variables based on piecewise linearization technique. Therefore, it is possible that with the change of the problem size, the quantity of segments used in the piecewise linearization method needs to be changed. However, other linearization processes utilized can be unchanged in most of the network.

Uncertainty modelling Uncertainty parameters

In the problem presented in the previous section, parameters such as energy price, γ , RESs power, P_R , load, P_C , Q_C , I_C , energy consumption required by EVs, TCE , charge rate of EVs, CR , apparent power control capacity, and harmonic currents of the EV chargers, \bar{S}_{EV} and \bar{I}_{EV} are uncertain. For scheduling of these resources, stochastic, probabilistic, or robust programming are used. But in stochastic and probabilistic programming, several different scenarios need to be applied to the problem, which leads to a slow convergence time. They also need to extract the probability distribution function (PDF) for any uncertainty parameter^{2,5}. This can also be extracted in implementing statistical studies for a long-term study period (for instance, one year), which takes so much time⁵. However, robust programming provides an appropriate modeling of unknown quantities in this work. Because the suggested issue only applies one case, it may be addressed much faster than using stochastic and probabilistic programming. Robust programming also removes the worst-case scenario brought on by the uncertainty. Therefore, a solution that is robust to prediction errors in the unknown parameters represents the optimal solution identified for the suggested design. Robust programming requires a variable matrix of uncertainties. Considering that the uncertainty matrix \bar{u} includes the forecasted values of the uncertainties, as specified in Eq. (39), the matrix of the uncertainty variable (u) can be written as the Eq. (40). The matrix has a number of rows equal to the number of buses (n_b). Also, the number of its columns (n_c) equals $n_c = (6 + n_h) \times n_t + 1$, where n_h and n_t represent the number of harmonics and operation hours, respectively. In Eqs. (39) and (40), γ in the first line has only one value, in other lines, its value is zero because according to Eq. (37), only the reference bus value has a value. Finally, the uncertainty set for the n -th row of the uncertainty matrix (U_n) is written as Eq. (41). In this regard, it indicates the deviation of uncertainty. UB stands for Uncertainty Budget, which is between [0, 1]. So that 0 represents the deterministic model, and UB≠0 illustrates the robust model. The term $[\bar{u} - \tilde{u}, \bar{u} + \tilde{u}]$ refers to the range of uncertainty changes. Term of “ \tilde{u} ” uncertainty deviation from \bar{u} .

$$\bar{u} = [P_C \ Q_C \ I_{C_{h=3}} \cdot I_{C_{h=n_h}} \ P_R \ CR \ \bar{S}_{EV} \ \bar{I}_{EV_{h=3}} \cdot \bar{I}_{EV_{h=n_h}} \ \gamma \ TCE] \tag{39}$$

$$u = [P_C^u \ Q_C^u \ I_{C_{h=3}}^u \cdot I_{C_{h=n_h}}^u \ P_R^u \ CR^u \ \bar{S}_{EV}^u \ \bar{I}_{EV_{h=3}}^u \cdot \bar{I}_{EV_{h=n_h}}^u \ \gamma^u \ TCE^u] \tag{40}$$

$$U_n = \left\{ \begin{aligned} & u_n \in R^{n_c} \mid \frac{1}{n_c} \sum_{i=1}^{n_c} \frac{|u_{n,i} - \bar{u}_{n,i}|}{\tilde{u}_{n,i}} \leq UB_n, \\ & \forall u_n \in [\bar{u}_{n,i} - \tilde{u}_{n,i}, \bar{u}_{n,i} + \tilde{u}_{n,i}] \end{aligned} \right\} \quad \forall n \tag{41}$$

The robust optimization of scheme

In this part of the article, adaptive robust optimization, also known as ARO, will be utilized to simulate the uncertainties. This method is capable of simultaneously extracting the most resilient ideal solution as well as the worst-case scenario. In this method, for a problem of $\min_{x \in \Gamma(x)} f(x)$, the worst-case scenario is obtained by adding $\max_{u \in U}$ to the problem. Therefore, the expression $\max_{u \in U} \min_{x \in \Gamma(x, u)} f(x, u)$ in proportion to the ARO objective simultaneously extracts the worst-case scenario and the robust solution represents the main problem variables such as power, voltage, and current in the proposed design. U denotes the sum of uncertainties, which is equal $\bigcup U_n$. $\Gamma(x)$ shows a set of problem constraints such as Eq. (37), and $f(x)$ is the objective function. The presence of the variable u in f and Γ in the robust model, $\max_{u \in U} \min_{x \in \Gamma(x, u)} f(x, u)$ is due to the dependence of the objective function and the constraint of the main problem on the value of the uncertainty variable. To solve this problem, we first extract the dual problem of $\min_{x \in \Gamma(x)} f(x)$, the details of which are presented in³⁵. The dual

formulation of the problem is $\max_{(\kappa, \omega) \in \Lambda(\kappa, \omega)} g(\kappa, \omega)$, where κ and ω represent the dual variables of equality and inequality constraints in $I(x)$, respectively. The set $\Lambda(\kappa, \omega)$ refers to the dual formulation constraints, and $g(\kappa, \omega)$ is the objective function of the duality problem. Extraction method of $\Lambda(\kappa, \omega)$ and $g(\kappa, \omega)$ for the problem $\min_{x \in I(x)} f(x)$ is presented in³³. In the following, the problem is stable as $\max_{u \in U} \max_{(\kappa, \omega) \in \Lambda(\kappa, \omega)} g(\kappa, \omega)$, which can be expressed as $\max_{u \in U, (\kappa, \omega) \in \Lambda(\kappa, \omega)} g(\kappa, \omega)$. This equation means that in the ARO method, the objective function of the robust model is equal to the duality of the objective function of the primary problem, $\min_{x \in I(x)} f(x)$, and its constraint equals the dual model of the constraint of the primary problem and the sum of uncertainties. Therefore, a robust model for the proposed design, (37)–(38), can be written as follows:

$$\begin{aligned} & \max \sum_i TCE_i^u \kappa_{PBi} + \\ & \sum_{n,o} \left(\begin{aligned} & P_{C_{n,o}}^u \kappa_{P_{n,o}} + Q_{C_{n,o}}^u \kappa_{Q_{n,o}} \\ & + \sum_{h,h \neq 1} \begin{pmatrix} I_{C_{n,o,h}}^u \kappa_{I_{n,o,h}} \\ + \bar{I}_{S_{n,h}} \bar{\omega}_{IS_{n,o,h}} \\ - \bar{I}_{S_{n,h}} \underline{\omega}_{IS_{n,o,h}} \\ + V_{h,o} \underline{\omega}_{V_{n,o,h}} \\ + \bar{V}_{h,o} \bar{\omega}_{V_{n,o,h}} \end{pmatrix} \\ & + \sum_v \left(\frac{\bar{V}_{h=1} - V_{h=1}}{n_v} \bar{\omega}_{\Delta V_{n,o,v}} \right) \\ & + \sum_m \left(z_n \bar{S}_{S_{n,o,m}} \bar{\omega}'_{SS_{n,o,m}} \right. \\ & \left. + \sum_l \bar{S}_{L_{n,l}} \bar{\omega}'_{SL_{n,l,o,m}} \right) \end{aligned} \right) + \\ & \sum_{i,o} \left(\begin{aligned} & P_{R_{i,o}}^u \kappa_{P_{V_{i,o}}} - P_{C_{i,o}}^u \kappa_{P_{V_{i,o}}} - Q_{C_{i,o}}^u \kappa_{Q_{V_{i,o}}} \\ & + \varpi_i P_{C_{i,o}}^u \bar{\omega}_{DR_{i,o}} - \varpi_i P_{C_{i,o}}^u \underline{\omega}_{DR_{i,o}} + CR_{i,o}^u \bar{\omega}_{PB_{i,o}} - \\ & \bar{S}_{EV_{i,o}} \underline{\omega}_{QE_{i,o}} + \\ & \sum_m \left(\bar{S}_{EV_{i,o}}^u \bar{\omega}'_{SE_{i,o,m}} \right. \\ & \left. + \left(\bar{S}_{R_{i,o}} - \right. \right. \\ & \left. \left. P_{R_{i,o}} \cos(m \times \Delta\varphi) \right) \bar{\omega}'_{SR_{i,o,m}} \right) + \\ & \sum_{h,h \neq 1} \begin{pmatrix} I_{C_{i,o,h}}^u \kappa_{IV_{i,o,h}} + \bar{I}_{R_{i,h}} \bar{\omega}_{IR_{i,o,h}} - \bar{I}_{R_{i,h}} \underline{\omega}_{IR_{i,o,h}} \\ + \bar{I}_{EV_{i,o,h}} \bar{\omega}_{IE_{i,o,h}} - \bar{I}_{EV_{i,o,h}}^u \underline{\omega}_{IE_{i,o,h}} \end{pmatrix} \end{aligned} \right) \\ & \forall z_n = 1 | n = s \end{aligned} \tag{42}$$

Subject to:

$$\begin{aligned} & \kappa_{P_{n,o}} + \sum_m \bar{\omega}'_{SS_{n,o,m}} \cos(m \times \Delta\varphi) \\ & = \omega_C \gamma_o^u + \omega_E : P_{S_{n,o}} \quad \forall n = s, o \end{aligned} \tag{43}$$

$$\begin{aligned} & \kappa_{Q_{n,o}} + \sum_m \bar{\omega}'_{SS_{n,o,m}} \sin(m \times \Delta\varphi) = 0 : Q_{S_{n,o}} \\ & \forall n = s, o \end{aligned} \tag{44}$$

$$\begin{aligned} & - \sum_n (J_{l,n} \kappa_{P_{n,o}}) + \kappa'_{PL_{n,l,o}} + \sum_m \bar{\omega}'_{SL_{n,l,o,m}} \cos(m \times \Delta\varphi) \\ & = 0 : P_{L_{n,l,o}} \quad \forall n, l, o \end{aligned} \tag{45}$$

$$\begin{aligned} & - \sum_n (J_{l,n} \kappa_{Q_{n,o}}) + \kappa'_{QL_{n,l,o}} + \sum_m \bar{\omega}'_{SL_{n,l,o,m}} \sin(m \times \Delta\varphi) \\ & = 0 : Q_{L_{n,l,o}} \quad \forall n, l, o \end{aligned} \tag{46}$$

$$\sum_n (I_{i,n} \kappa_{P_{n,o}}) + \kappa_{PV_{i,o}} = \omega_E \sum_n I_{i,n} : PV_{i,o} \quad \forall i, o \tag{47}$$

$$\sum_n (I_{i,n} \kappa_{Q_{n,o}}) + \kappa_{QV_{i,o}} = 0 : Q_{V_{i,o}} \quad \forall i, o \tag{48}$$

$$-\kappa_{PV_{i,o}} + \underline{\omega}_{DR_{i,o}} + \bar{\omega}_{DR_{i,o}} + \kappa_{DR_{i,o}} = 0 : P_{DR_{i,o}} \quad \forall i, o \tag{49}$$

$$\begin{aligned} \kappa_{PV\ i,o} + \kappa_{PE\ i,o} - a_i \kappa'_{PLO\ i,o} + \sum_m \bar{\omega}'_{SE\ i,o,m} \cos(m \times \Delta\varphi) \\ \leq 0 : P_{EV\ i,o} \quad \forall i, o \end{aligned} \tag{50}$$

$$\begin{aligned} \kappa_{QV\ i,o} + b_i \kappa'_{PLO\ i,o} + \underline{\omega}_{QE\ i,o} + \sum_m \bar{\omega}'_{SE\ i,o,m} \sin(m \times \Delta\varphi) \\ \geq 0 : Q_{EV\ i,o} \quad \forall i, o \end{aligned} \tag{51}$$

$$-\kappa_{PE\ i,o} + \kappa_{PB\ i} + \bar{\omega}_{PB\ i,o} \leq 0 : P_{B\ i,o} \quad \forall i, o \tag{52}$$

$$-\kappa_{PE\ i,o} + \kappa'_{PLO\ i,o} \leq 0 : P_{LO\ i,o} \quad \forall i, o \tag{53}$$

$$-\kappa_{QV\ i,o} + \sum_m \bar{\omega}'_{SR\ i,o,m} \sin(m \times \Delta\varphi) = 0 : Q_{R\ i,o} \quad \forall i, o \tag{54}$$

$$\begin{aligned} \kappa_{I\ n,o,h} + \bar{\omega}_{IS\ n,o,h} + \omega_{IS\ n,o,h} = 0 : I_{S\ n,o,h} \\ \forall n = s, o, h \neq 1 \end{aligned} \tag{55}$$

$$\begin{aligned} -\sum_n (J_{l,n} \kappa_{I\ n,o,h}) + \kappa_{IL\ n,l,o,h} = 0 : I_{L\ n,l,o,h} \\ \forall n, l, o, h \neq 1 \end{aligned} \tag{56}$$

$$\sum_n (I_{i,n} \kappa_{I\ n,o,h}) + \kappa_{IV\ i,o,h} = 0 : I_{V\ i,o,h} \quad \forall i, o, h \neq 1 \tag{57}$$

$$-\kappa_{IV\ i,o,h} + \underline{\omega}_{IR\ i,o,h} + \bar{\omega}_{IR\ i,o,h} = 0 : I_{R\ i,o,h} \quad \forall i, o, h \neq 1 \tag{58}$$

$$-\kappa_{IV\ i,o,h} + \underline{\omega}_{IE\ i,o,h} + \bar{\omega}_{IE\ i,o,h} = 0 : I_{EV\ i,o,h} \quad \forall i, o, h \neq 1 \tag{59}$$

$$\begin{aligned} \underline{\omega}_{V\ n,o,h} + \bar{\omega}_{V\ n,o,h} - \sum_l Y_{L\ n,l,h} \kappa_{IL\ n,l,o,h} \\ \leq \omega_T : V_{n,o,h} \quad \forall n, o, h \neq 1 \end{aligned} \tag{60}$$

$$\bar{\omega}_{\Delta V\ n,o,v} - G_{L\ n,l,h=1} \left(\sum_v \left(\begin{matrix} slop_v^- \\ V_{h=1}^- \\ -V_{h=1}^- \end{matrix} \right) \kappa'_{PL\ n,l,o} \right) \tag{61}$$

$$+ B_{L\ n,l,h} = \left(\sum_v \left(\begin{matrix} slop_v - V_{h=1}^- \\ -V_{h=1}^- \end{matrix} \right) \kappa'_{QL\ n,l,o} \right) \leq 0 : \Delta V_{n,o,v}, \forall n, o, v$$

$$z_n \kappa_{\beta n,o} + \left(V_{h=1}^- \right)^2 \sum_l \left(\begin{matrix} B_{L\ n,l,h=1} \kappa'_{PL\ n,l,o} + \\ G_{L\ n,l,h=1} \kappa'_{QL\ n,l,o} \end{matrix} \right) \tag{62}$$

$$= 0 : \beta_{n,o} \quad \forall n, o, z_n = 1 | n = s$$

$$\kappa \in (-\infty, +\infty), \omega \leq 0, \bar{\omega} \geq 0 \tag{63}$$

$$u \in \bigcup_n U_n \tag{64}$$

Equation (42) displays the robust problem’s objective function based on ARO, which is the same as the objective function’s dual formulation in Eq. (37). The dual formulation of constraints (43)–(62) is derived from the variables of the primary issue (voltage, power, and current), where the primary variable associated with each constraint follows the phrase “:”. Finally, constraint (64) reveals the restriction of the variables of uncertainty. Constraint (63) also shows the limitation of the variables of the dual issue. In addition, whereas constraints in problems (42)–(64) have linear relationships, the objective function has two continuous variables multiplied by them. But because it’s a convex issue, there are several ways to solve it and an ideal solution. Additionally, this issue may be effectively solved using linear programming (LP) solvers like CPLEX. Finally, the problem-solving process is illustrated in the flowchart shown in Fig. 2.

The proposed scheme is formulated in mathematical form. It is an optimization problem. This problem has an objective function. In the objective function, the minimum and maximum of an economic or technical function are calculated. In other words, the objective function has the min and max expression. The optimization problem also has constraints. The constraints appear as equal and unequal equations. To apply the optimization model to the distribution network, an intelligent platform is required. The smart scheme includes intelligent algorithms and telecommunication devices .

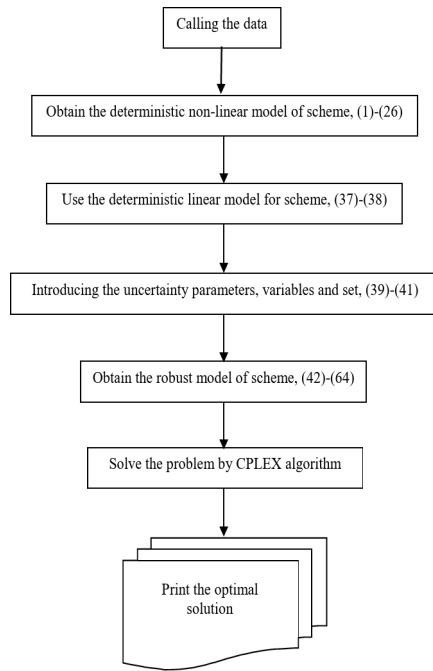


Fig. 2. Flowchart illustrating the problem-solving process.

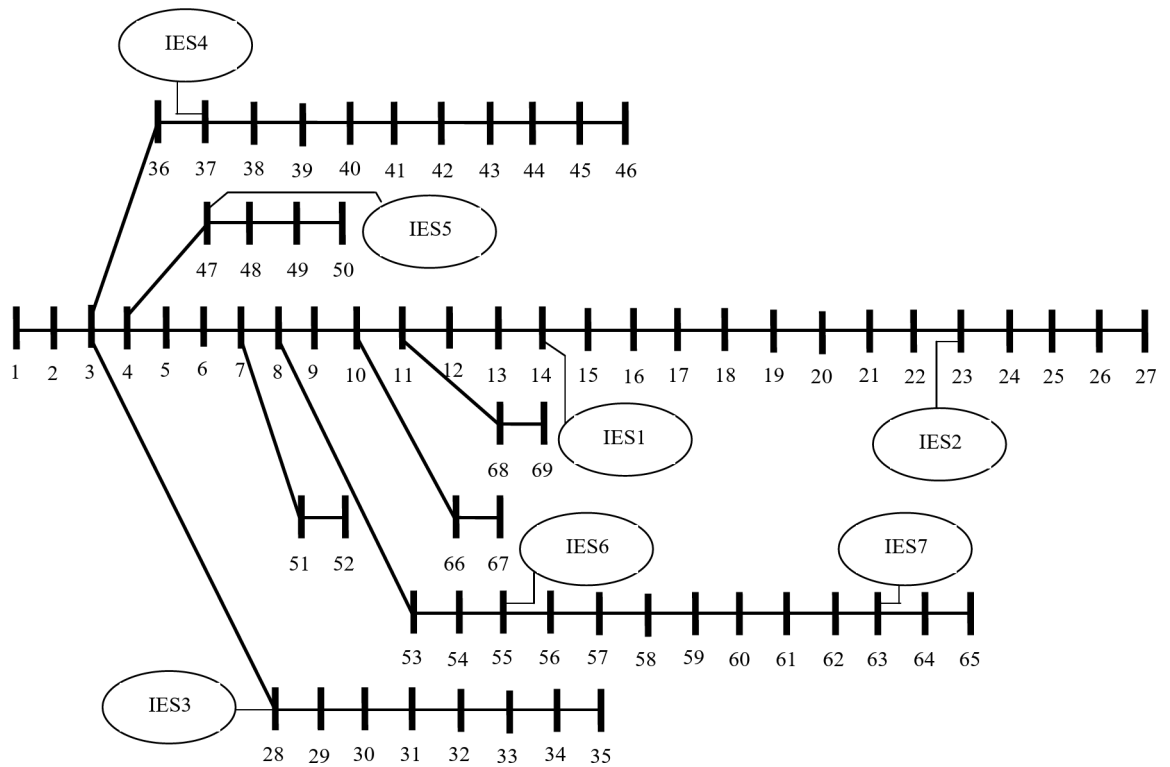


Fig. 3. IEEE 69 bus SDN in the presence of FRIESSs.

Numerical results and discussion

Case study

Figure 3 shows the previously proposed system evaluated on the IEEE 69-bus radial SDN. The base power and voltage for the test network are 1 MVA and 12.66 kV, respectively. This network's distribution substations. Peak load data is taken from in several busses, and hourly load data is obtained by multiplying the daily load factor

curve by the peak load. This curve is shown in Fig. 4. The purchase prices of energy for SDN in three periods of low load, medium load and high load are \$16/MWh, \$24/MWh and \$30/MWh. It is recommended to keep the voltage range of the buses in the main frequency component within the range of [0.9 1.05] per unit. The off-peak load period is between 1:00 and 7:00, and the peak load period is between 17:00 and 22:00. Other hours also represent mid-peak load. In this network, nonlinear loads with 6-pulse rectifier type are installed in 9, 16, 33, 46, 51, 62 and 69 buses. Note that the harmonic current of the load ($h \neq 1$) is a factor of the apparent power of the load, i.e. These loads have individual harmonics between 5 and 43, the harmonic coefficient θ for this number of harmonics is reported in³⁴. Also, the allowable current passing through the distribution substation in the harmonic frequency component for the voltage level of 12.66 kV is determined according to IEEE519 standard, which is available in³⁶ of this standard. According to this standard, the maximum harmonic voltage range is equal to 3% or 0.03 per unit. In the network mentioned in this section, seven FRIESSs are used, whose position is specified in Fig. 3, and their peak load data are reported. At each FRIES, consumers involvement rate in the DRP is 50%. FRIESSs 1, 2, 6 and 7 have WT and PV systems with a size of 0.3 MVA, and other FRIESSs have a capacity of 0.5 MVA for RESs. The electronic converter capacity of the power of RESs in each harmonic ($h \neq 1$), i.e. is equal to 5% of. Also, the hourly data of the active power output of RESs (P_R) is the product of \bar{S}_R and the daily power rate curve of RESs, as shown in Fig. 4 for the WT and PV systems³⁴. In FRIESSs 3–5, up to 200 EVs can receive their required from the FRIESS, but up to 150 EVs in other FRIESSs can be deployed. The number of EVs for each FRIES is determined by multiplying the total number of EVs in the FRIESSs and the EV penetration rate. The daily infiltration rate curve of EVs is presented in Fig³⁴. The charger loss coefficients of EVs, i.e. a and b , have values of 0.09 and 0.0475, respectively, and other characteristics of EVs such as charge rate, charger capacity, the energy consumption required per EV have been reported in². In each harmonic, the amount I_{EV} is equal to 5% of \bar{S}_{EV} . There is no nonlinear load in FRIESSs, so the I_C is zero.

In this article, the capacity of power converters in the path of electric vehicles and renewable sources is generally considered to be more than their maximum active power. For example, the data of vehicles is selected from³⁴. In these references, the maximum active power of the vehicle is equal to kW, while the charger capacity is equal to 4.6 kVA. Therefore, vehicle chargers have free capacity to control reactive power and compensate harmonics. In addition, based on Fig. 4, renewable resources generally have less active power than their capacity. Only in the hours when the amount of active power generation of sources is high, their capacity to control reactive and harmonic power decreases. Moreover, there are up to 7 IES in the network based on Fig. 3. These IES have 1200 electric vehicles. Based on the data stated for electric vehicles, the minimum capacity of chargers to control reactive power and harmonics is around 3 to 3.5 MVar. The minimum capacity of converters in the path of renewable resources to control reactive and harmonic power based on the data of subsection IV.A is around 1 to 1.5 MVar. Therefore, the capacity of IES to control reactive power and harmonics is around 4 to 5 MVar. In addition to this, the proposed problem model can be implemented across various distribution networks, resources, and active loads. Only by changing the size of the problem, it is necessary to change the setting parameters in the linearization techniques. In other words, if the volume of the problem increases, the number of line segments increases, and the circular plane is approximated as a regular polygonal plane with more sides. Finally, time step is considered 1 h, but, the proposed problem does not have a limit to consider implementation steps lower than 1.

Results

The present section involves the execution of the proposed problem within the GAMS software framework. Subsequently, the proposed robust linearized problem (37)-(38) is solved by utilizing the CPLEX solver. In this problem, five segments are employed in the conventional piecewise linearization method. Additionally, a circular plane is approximated as a regular 45-sided polygon³⁴. In this section, as in^{2,6,34}, the uncertainty deviation (\bar{u}) is equalized to $UL \times UB \times \bar{u}$, which UL represents the level of uncertainty.

Finding a proper solver for the suggested scheme

Table 2 presents the Pareto front for the proposed design in the deterministic model (level of uncertainty equal to zero or $v=0$), which is extracted for four values of each weighting coefficient, i.e. 0, 0.33, 0.5 and 1. For the

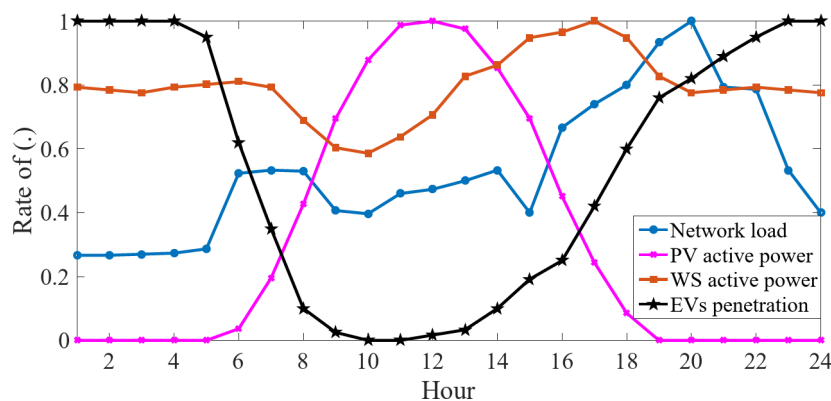


Fig. 4. Daily load factor curve, RESs power rate, and EV penetration rate.

ω_C	ω_E	ω_T	Cost (\$)	EL (MWh)	SHV (p.u.)
1	0	0	723.5	1.892	158.9
0	1	0	831.6	1.426	137.7
0	0	1	892.2	1.731	95.3
0.5	0.5	0	779.6	1.545	156.4
0.5	0	0.5	802.7	1.672	103.1
0	0.5	0.5	845.8	1.522	101.3
0.33	0.33	0.33	791.1	1.563	106.5

Table 2. Pareto front in the final model of the proposed design.

Model	Solver	Total number of equations/variables	ω_C	ω_E	ω_T	Cost (\$)	EL (MWh)	SHV (p.u.) – TVT	CT (s)	CI
NLP	IPOPT	295,723 / 491,107	0.11	0.74	0.15	762.8	1.534	109.8–39.3	793.5	127
	CONOPT	295,723 / 491,107	0.12	0.72	0.16	778.3	1.547	113.6–40.4	905.4	422
	OQNLP	Infeasible solution								
	DISOPT	295,723 / 491,107	0.12	0.71	0.17	791.5	1.565	118.3–41.5	1094.7	519
	KNITRO	Infeasible solution								
LP	CPLEX	312,709 / 517,204	0.11	0.73	0.16	753.4	1.514	105.6–38.5	20.3	95
	CBC	312,709 / 517,204	0.11	0.73	0.16	753.4	1.514	105.6–38.5	26.7	161
	CONOPT	312,709 / 517,204	0.11	0.73	0.16	753.4	1.514	105.6–38.5	31.4	278

Table 3. Compromise solution in the final model of the proposed design obtained from different solvers.

coefficients $\omega_C=1$, $\omega_E=1$ and $\omega_T=1$, the lowest and highest values of the objective functions as *Cost*, *EL* and the sum of the harmonic voltage (*SHV*), $\sum_{n,o,h \neq 1} V_{n,o,h}$, can be calculated. As per Table 2, the minimum and maximum values for the *Cost* are \$723.5 and \$8.292, respectively. These values for *EL* (*SHV*) are 1.4266 MWh (95.3 p.u.) and 1.892 MWh (158.9 p.u.), respectively. The range of variations for a target function on the Pareto front is known as the variance between the highest and lowest values of that function. Hence, the range of changes in *Cost*, *EL*, and *SHV* are respectively \$168.7, 0.466 MWh, and 6/63 p.u. Also, Table 2 shows that the changing direction of each objective function does not align in the same direction. For example, the increase in energy losses (fifth column) is proportional to the reduction in network operation costs (fourth column). This is because it is critical for environmentally friendly resources with low operating costs, like as FRIESS, to pump high active power into the grid to lower energy prices. In this instance, however, the substation line flow from FRIES to the upstream network may rise as compared to load flow studies (network without FRIES). The losses in substation lines would grow, as would the network’s power and energy losses. Also, note that the only sources of harmonic control in FRIES are RESs and EVs aggregation. In case of cost reduction, it is necessary to inject high active power from these sources. But this will reduce the ability of these components to control reactive power and harmonic current. Therefore, the cost reduction follows the *SHV* escalation. These conditions also are true between *EL* and *SHV*. Table 3 tabulates the reports of the compromise solution extracted from the Pareto front using the fuzzy decision approach. Note that in this table, the results obtained from the two models of nonlinear programming (NLP), (1)-(26), and linear programming (LP), (37)-(38), are presented for the proposed design. Furthermore, solvers like IPOPT, CONOPT, OQNLP, DISOPT and KNITRO are used for NLP, and CPLEX, CBC and CONOPT solvers are used for LP. Table 3 shows that the NLP model’s OQNLP and KNITRO solvers are unable to provide an ideal answer. Not only might other NLP algorithms not provide a unique answer, but they can produce varied results. Out of all of these algorithms, the IPOPT solver has been able to outperform CONOPT and DISOPT in terms of efficiency and convergence speed. So that the values of *Cost*, *EL* and *SHV* (TVT) in the compromise solution for IPOPT is smaller than CONOPT and DISOPT. It also has a lower computational time (CT) and convergence iteration (CI) than CONOPT and DISOPT, resulting in a higher convergence speed than other NLP solvers. However, according to Table 3, it can be seen that LP solvers have been able to obtain an optimal and unique solution, so that the values of *Cost*, *EL* and *SHV* (TVT) in these solvers have the lowest values compared to those of IPOPT solver. Even though the LP has a greater number of equations and variables compared to NLP, the computational time of these solvers is much reduced compared to even the best NLP solver, IPOPT. As a point, in non-convex nonlinear problems, a suitable solver among the others has a solution with more optimality and lower computational time. This is observed in the CPLEX algorithm based on Table 3. Because the minimum value of different objective functions and lower computational time are observed in this solver than other solvers. In addition, it is noted that the trade-off point is different for NLP solution algorithms, as the best solution for these algorithms is different. But these conditions are not observed in LP solvers. Tables 2 and 3 may be compared to determine that the values of the *SHV*, *EL*, and *Cost* the functions at the trade-off point are near their minimum values points. Accordingly, the compromise point’s cost function, as compared to its lowest point, is around 17.7% ((723.5–753.4)/168.7); the 168.7 represents the cost function’s fluctuating range. For *EL* and *SHV*, this figure is 18.8% and 22.8%, respectively.

Evaluation of robust compromise solution

Figure 5 shows the objective functions of *Cost*, *EL*, and *TVT* at the compromise point in terms of the level of uncertainty (UL) for varying uncertainty budget (UB). As the figure illustrates, by increasing UL at UB=0, the mentioned objective functions do not alter. Because in this instance, the variation in the uncertainty parameter consistently remains at zero, i.e. UB=UL=0, hence the ensuing scenario will be equivalent to the scenario related to the deterministic model. Consequently, in return for a change in the degree of uncertainty, the values of the various objective functions will remain constant. But in the case of UB=0.5 (UB=1), increasing

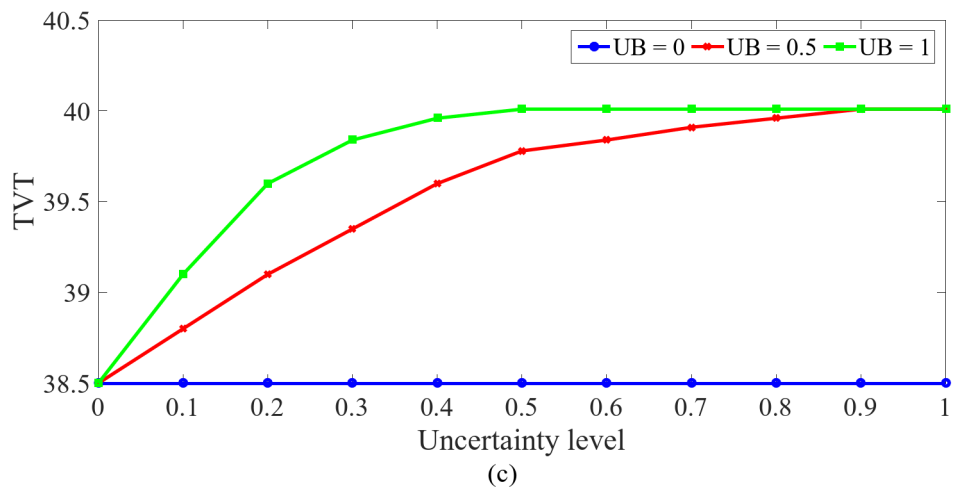
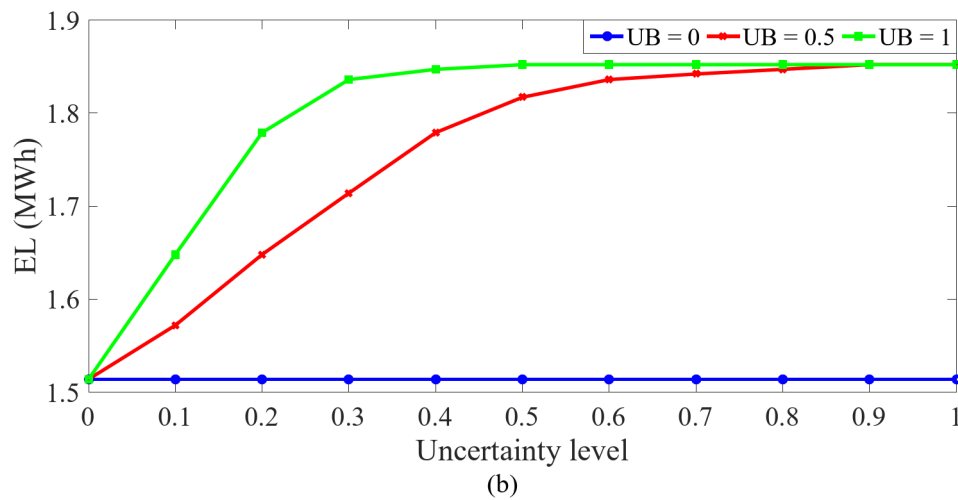
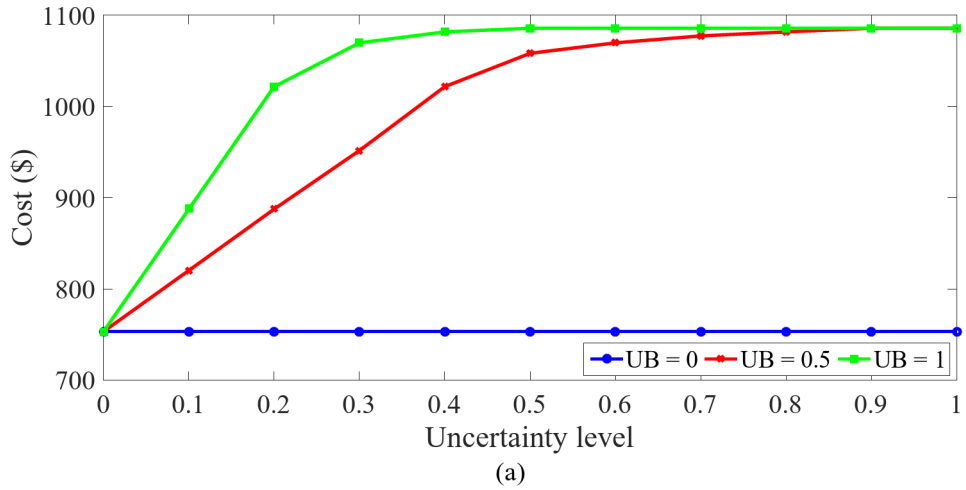


Fig. 5. Value of objective functions in uncertainty level, (a) Cost, (b) EL, and (c) TVT for varying uncertainty budget.

UL to 0.9 (0.5), the value of the mentioned objective functions increases. This is because, according to Table 4, the increase in the level of UL cause to rise in load, P_C , Q_C and I_C , energy price, γ , energy consumption of EVs, TCE , and decreases the production capacity of RESSs, P_R , charging rate of EVs, C_R , the capacity of the EV charger to control reactive power and harmonic current, \bar{S}_{EV} and \bar{I}_{EV} in the worst-case scenario, the ratio of the scenario associated with the model becomes deterministic. So in the worst-case scenario, the energy demand and price increase while the energy production decreases. Therefore, raising the level of uncertainty leads to an increase the $Cost$, EL and TVT in the robust model relative to the deterministic design approach. Nevertheless, for $UL > 0.9$ ($UL > 0.5$) at $UB = 0.5$ ($UB = 1$), the values of the functions is saturated and their values are constant and equal to the case results $UL = 0.9$ ($UL = 0.5$). This suggests that by considering the high values for UL and UB, energy price and energy demand (energy production capacity) may acquire the highest rise (reduction) in the worst-case scenario compared to the scenario associated with the deterministic model. Thus, the solution obtained in these conditions will have the most robust optimal point. This indicates that the suggested design with optimal power management of FRIESs in the network can achieve a maximum deviation of uncertainty (forecast error) of 45% ($UL \times UB = 0.9 \times 0.5 \times 100$) due to load uncertainties. The price of energy, RESSs active power, and energy consumption of EVs should be resilient and be able to find an optimal solution. According to Sect. 3.3, and²³, the worst-case scenario has less solution region than the scenario related to the deterministic model. So, this takes so much time in the robust model compared to the deterministic model. According to Table 4, with increasing UL and UB, the computational time is longer than that of the deterministic model ($UL = UB = 0$). Note that these conditions are up to $UB = 0.5$ and $UL = 0.9$.

In the proposed approach, from a financial perspective, the cost framework for the energy acquired by the distribution network from the upstream network is presented as Eq. (1). The results of this cost are shown in Tables 2 and 3; Fig. 5(a). In Fig. 5, the cost for different robust models is presented. The cost difference between the point $UL = 0$ (deterministic model) and $UL \neq 0$ (robust model) depicts the expenses associated with upgrading the distribution network to address uncertainties related to load demand, energy prices, renewable energy sources, and electric vehicles.

The operating condition of FRIES

Figure 6 illustrates the daily profile of the active power for FRIESs and their components for different levels of uncertainty at $UB = 1$. According to Fig. 6(a), it can be seen that in the definite model ($UL = 0$), FRIESs are energy consumers at 1:00–6:00, but at other times they are the producers in the SDN. At 1:00–6:00, according to Sect. 4.1, the energy price has the lowest value, i.e. \$16/MWh, compared to the other hours. Therefore, to minimize the cost, EVs as shown in Fig. 6(b) provide the energy consumption needed for their travel in the coming hours. In other hours, the active power of EVs will be equal to the charger losses due to reactive power control. Additionally, the largest energy price is seen between 17:00 and 22:00, which is peak hour. Therefore, it is expected that customers who participate in DRP would reduce their energy use during times of high demand, as illustrated in Fig. 6(c), as well as during peak and mid-peak hours, in order to attain the minimal cost value. Figures 4 and 6(d) show that the PV system is able to pump active power into the FRIES at other times, but it is not able to create active power between 1:00 and 6:00 and 19:00 and 24:00. WT system may additionally inject 60–100% of its active power into the FRIES at all simulation hours according to Figs. 4 and 6(e). In accordance with this RES and flexibility function, FRIESs are considered energy producers outside of the hours of 1:00–6:00 and consumers during that time. Thus, compared to other hours, a considerable amount of active power is fed into the SDN during the hours of 8:00 and 19:00. Additionally, as seen in Fig. 6(a), the number of hours that FRIESs are using will exceed that of the deterministic model ($UL = 0$) as uncertainty increases. Table 4 indicates that under these circumstances, EVs' charge rates drop; as a result, EVs demand more active power from the network to recharge their batteries over extended hours, as shown in Fig. 6(b). Additionally, when UL increases, the active power curve of FRIESs moves downward in comparison to the deterministic model, as seen in Fig. 6(a). So they get more active power than the typical SDN model during the corresponding hours of usage. Additionally, they inject less active power into the SDN during these hours of generation than they would when

UB	0				0.5			1		
UL	0	0	0.1	0.2	0	0.1	0.2	0	0.1	0.2
Sum of γ^u (\$/MWh)	550	550	577.5	605	550	605	660	550	605	660
Sum of P_C^u (MW)	68.9	68.9	72.3	75.8	68.9	75.8	82.7	68.9	75.8	82.7
Sum of Q_C^u (MVar)	32.3	32.3	33.9	35.5	32.3	35.5	38.8	32.3	35.5	38.8
Sum of I_C^u (A)	1.053	1.053	1.106	1.158	1.053	1.158	1.264	1.053	1.158	1.264
Sum of P_R^u (MW)	71.8	71.8	68.2	79	71.8	79	86.2	71.8	79	86.2
Sum of TCE^u (MWh)	11.52	11.52	12.1	12.67	11.52	12.67	13.82	11.52	12.67	13.82
Sum of CR^u (MW)	3.6	3.6	3.42	3.24	3.6	3.24	2.88	3.6	3.24	2.88
Sum of \bar{S}_{EV}^u (MVA)	5.52	5.52	5.24	4.97	5.52	4.97	4.42	5.52	4.97	4.42
Sum of \bar{I}_{EV}^u (A)	0.276	0.276	0.262	0.248	0.276	0.248	0.221	0.276	0.248	0.221
CT (s)	20.3	20.3	21.4	22.6	20.3	22.6	24.7	20.3	22.6	24.7

Table 4. Value uncertainties parameter and calculation time in the worst-case scenario for different value of UL and UB.

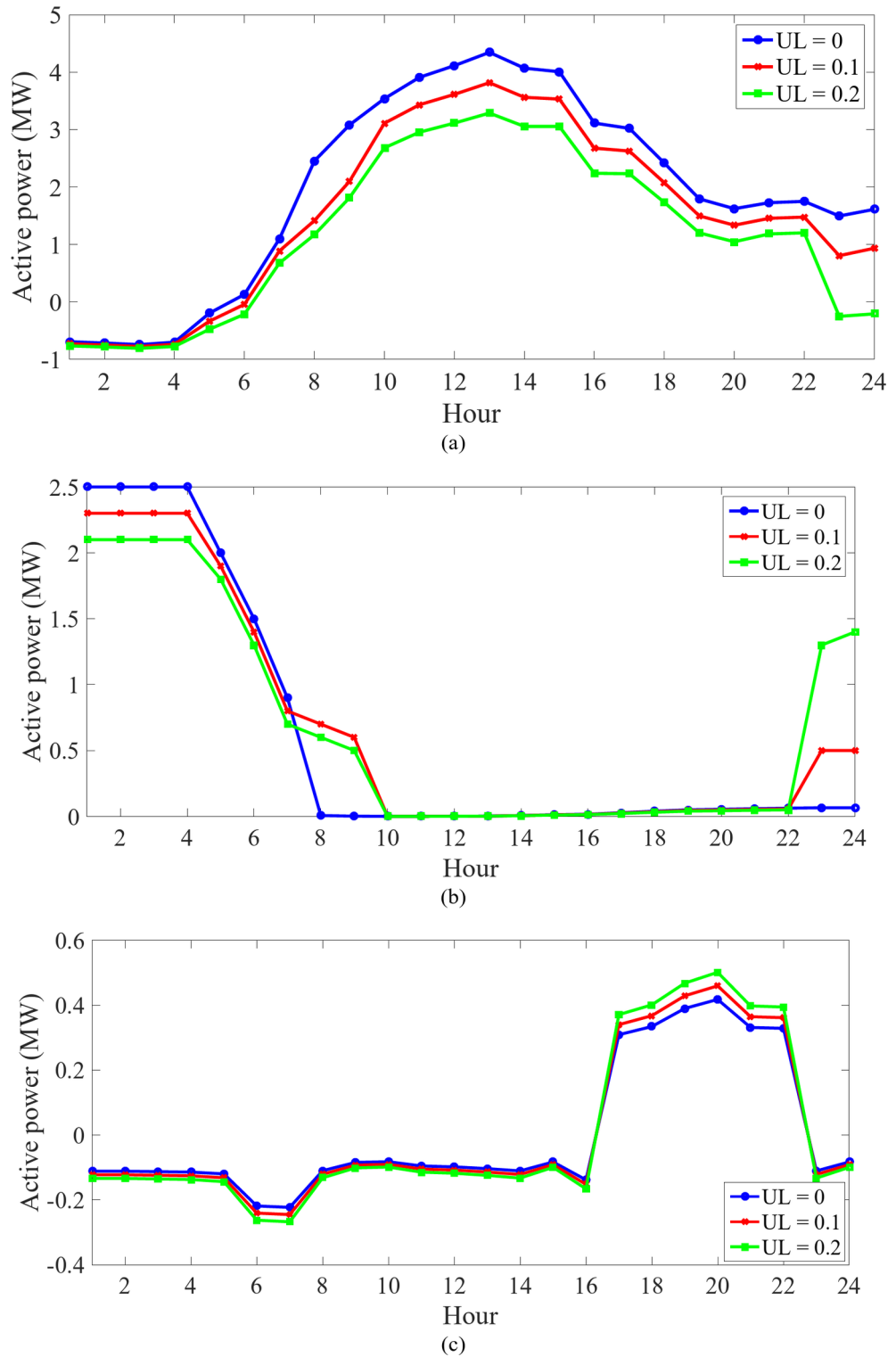


Fig. 6. Daily active power curve of, (a) FRIESS, (b) EVs, (c) DRPs, (d) PVs, and (e) Ws for different value UL in UB=1.

UL=0. This is as a result of the worst-case scenario's higher energy consumption and lower energy output as compared to the scenario with UL=0, as shown in Table 4; Fig. 6(b)–6(e).

Figure 7 displays the daily reactive power curves for the EVs and RESs, the reactive power control components, and the FRIESS for various UL values at UB=0. Keep in mind that lowering the voltage drop between the buses is essential to lowering grid energy losses. As a result, injecting FRIESS' reactive power will successfully lower voltage loss. In Fig. 7(a), this curve is shown. Electronic power converters for RESs and EV chargers make up the

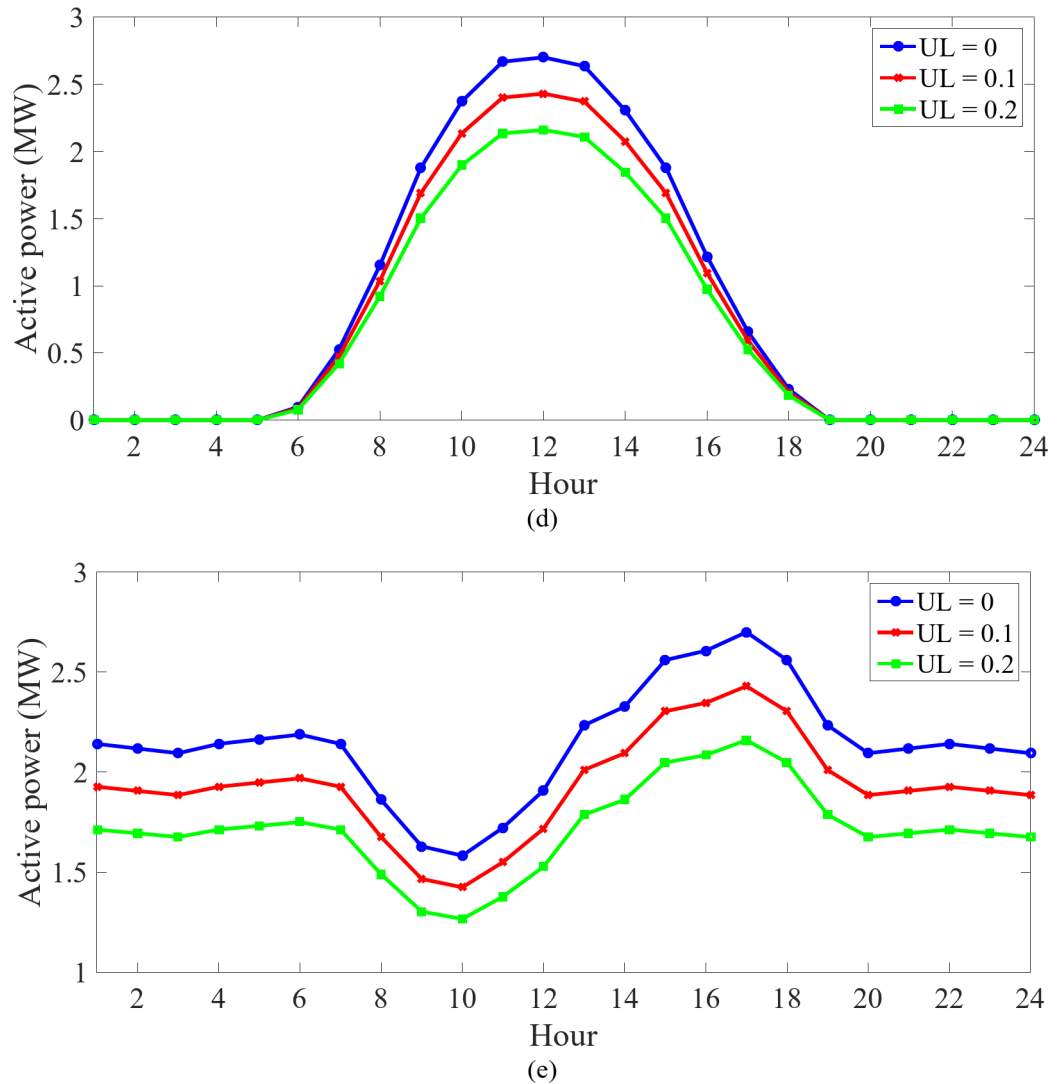


Figure 6. (continued)

reactive power control components of the FRIES. The daily curve of reactive power injection of EVs to FRIES shown in Fig. 7(b) has the same trend as the daily rate of EV penetration rate in Fig. 3 because the number of EVs per hour changes as shown in Fig. 3. Additionally, Eq. (17) states that the quantity of active power generated by RESs determines their ability to regulate reactive power. As a result, when the RESs' active power is increased as shown in Fig. 6(d) and 6(e), their ability to manage reactive power is diminished, which lowers the reactive power of the RESs as shown in Fig. 6c and d. Consequently, Fig. 7(a) will provide the daily reactive power curve of FRIESs. They pump more reactive power into the SDN between the hours of 1:00–6:00 and 23:00–24:00. Because a significant number of EVs are connected to FRIESs during these times, the active power production of the RESs is lower than during other hours, as shown in Fig. 6(d) and 5(e). As a result, EVs and RES based on Fig. 7(b) – 7(d) may provide substantial reactive power to FRIESs during these hours. At times, however, the amount of EVs falls while the active power of the RESs grows. So they inject less reactive power into the FRIESs from 1:00–6:00 and 23:00–24:00. Note that FRIESs have been able to appear in the SDN as reactive power generators at all hours. Figure 7 shows that the increase in UL in the most unfavorable scenario, compared to the deterministic model scenario where uncertainties are zero ($UB = UL = 0$), there is a reduction in the reactive power injection from FRIESs during certain hours of 1:00–8:00 and 18:00–24:00 (9:00–17:00). This is due to the following reasons: (1) According to Table 4, by increasing the value of UL, \bar{S}_{EV} decreases accordingly, hence, the capacity of EV chargers in reactive power control decreases. (2) By increasing UL, in the worst-case scenario, the active power output from the renewable energy sources (RESs) decreases, which in turn reduces their capacity to manage reactive power increases. According to Fig. 7(b)–7(d), EVs have higher reactive power than RES at 1:00–8:00 and 18:00–24:00. Therefore, the reactive power of FRIESs decreases in these hours in exchange for an increase in UL which is due to a decrease in the capacity of EVs to control reactive power. The reactive power of RESs is higher than that of EVs at 9:00–17:00. Therefore, the increase in reactive power of FRIESs during these hours is due to the increase in UL and the increase in RES capacity in reactive power control.

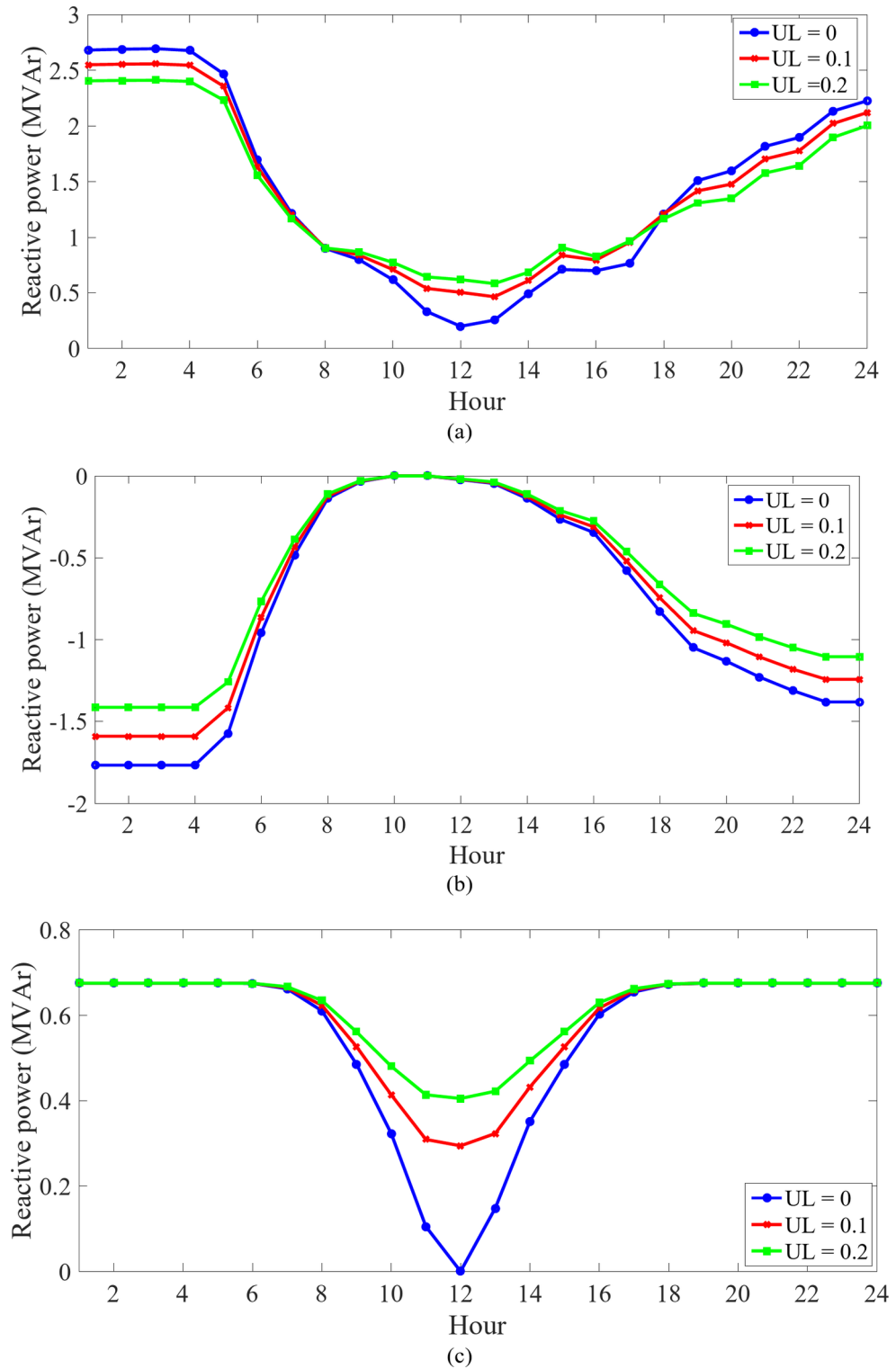


Fig. 7. Daily reactive power curve of, (a) FRIESs, (b) EVs, (c) PVs, and (d) WSs for different value of UL in UB=1.

The effective daily harmonic flow curve for all FRIESs and harmonic control sources, i.e. RESs and EVs, for different ULs and UB=1 is shown in Fig. 8. The effective harmonic current for the 1st FRIES at 0 is calculated

as $I_{RMS\ i,o} = \sqrt{\sum_{h \neq 1} (I_{V\ i,o,h})^2}$. When UL=0, as depicted in Fig. 8(a), the pattern of temporal variations in

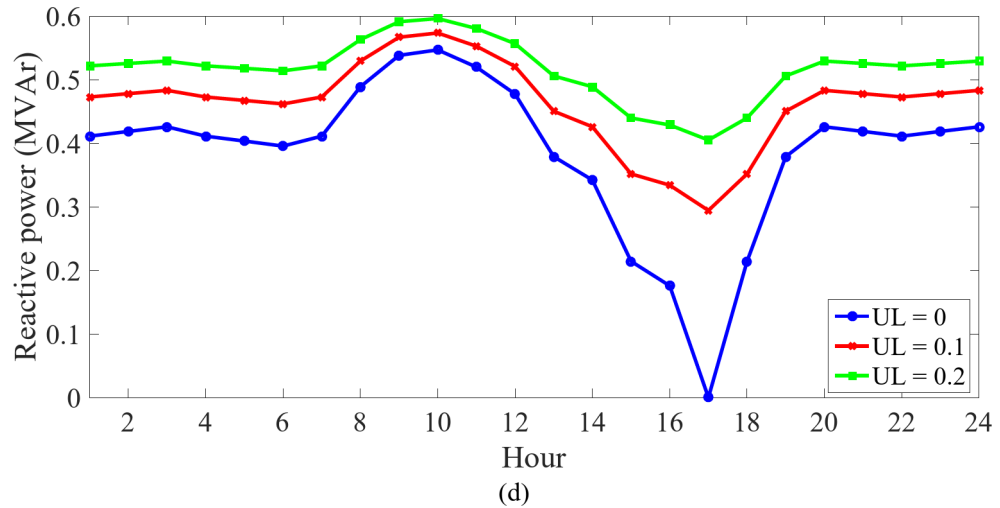


Figure 7. (continued)

the harmonic current of FRIESs mirrors the trend observed in the load coefficient changes shown in Fig. 4. Because the harmonic current of nonlinear consumers was considered as a factor of their apparent power consumption according to Sect. 4.1. Therefore, FRIESs are expected to compensate for the high percentage of harmonic currents of nonlinear consumers during all operating hours to achieve the minimum value of *SHV* or *TVT*. So the effective harmonic current time curve of FRIESs will be almost similar to the load factor curve. Note, however, that the capacity of EVs to control harmonic current depends on the quantity of EVs connected to the FRIES during each hour. Therefore, the effective harmonic current of the EVs as in Fig. 8(b) will have a daily curve similar to the trend shown in the EV penetration rate in Fig. 4. However, RESs can have an effective harmonic flow curve similar to the daily load coefficient curve in Fig. 4, and in addition, it should be noted that based on Fig. 8, we can say that the effectiveness of RESs in controlling the harmonic current is greater than EVs, because their daily harmonic current curve (RESs and FRIESs) are close to each other. Note that the increase in UL has caused the effective harmonic current curve of FRIESs to shift upwards, according to Fig. 5(c). This is due to the fact that under these conditions, the harmonic current of nonlinear consumers increases according to Table 4, so it is expected that the harmonic current of FRIESs to offset the harmonic currents generated by nonlinear loads will increase compared to UL=0. This will be the same as in Fig. 8(c) due to the increase in RESs harmonic current because the rate decreases by increasing UL according to Table 4; Fig. 8(b).

Assessing the performance and power levels quality of SDN

To investigate the impacts of the suggested approach to operating conditions and power quality (harmonic), the following five studies are performed:

- Case study 1: SDN load flow study (network without FRIES).
- Case study 2: Proposed design considering only RESs in FRIES.
- Case Study 3: Proposed design considering only DRPs in FRIES.
- Case study 4: Proposed design considering only EVs in FRIES.
- Case study 5: Implementing the proposed design.

Table 5 reports the results for UB=1. According to this table, it can be seen that RESs and DRPs are able to reduce energy losses alone by adopting a suitable power management system in the proposed scheme, but EVs do not have such a capability. So that the reduction percentage of this utilization index by RESs is higher than DRPs. Because RESs are the only injectors of active and reactive power to FRIES or SDN. As a result, under these settings, the power and energy sought from the upstream network are lower than in the first example, resulting in lower energy losses. However, DRP just transfers peak energy use to off-peak and mid-peak hours. Because EVs use energy, their presence in the grid will raise the power demand from the upstream grid, resulting in a rise in SDN energy losses. In the voltage profile (an operating index), DRPs and EVs in the third and fourth cases reduced the maximum voltage drop of 0.092 per unit in the first case to 0.064 and 0.057 per unit in the worst-case scenario (UL=0.2) without causing overvoltage. However, RESs have caused a maximum overvoltage of 0.012 per unit in the SDN to reduce the maximum voltage drop to 0.049 per unit at UL=0.2. RESs inject active and reactive power into the grid simultaneously, EVs can only inject reactive power into the SDN, and DRP shifts energy from peak-load period to off-peak and mid-peak periods. Therefore, priority is with RES, then EVs, and finally with DRPs for improving the voltage profile. Regarding the power factor of the substation, it should be said that RESs and EVs are always able to control the reactive power in the second and fourth cases to UB=1 according to Fig. 7, which is more than 0.9 even in the worst-case scenario (UL=0.2). But this has not been achieved in the third case (presence of DRPs alone in FRIESs), so the minimum power factor at UL=0.2 is equal to 0.885. Nevertheless, it has been able to improve or upgrade this coefficient compared to the

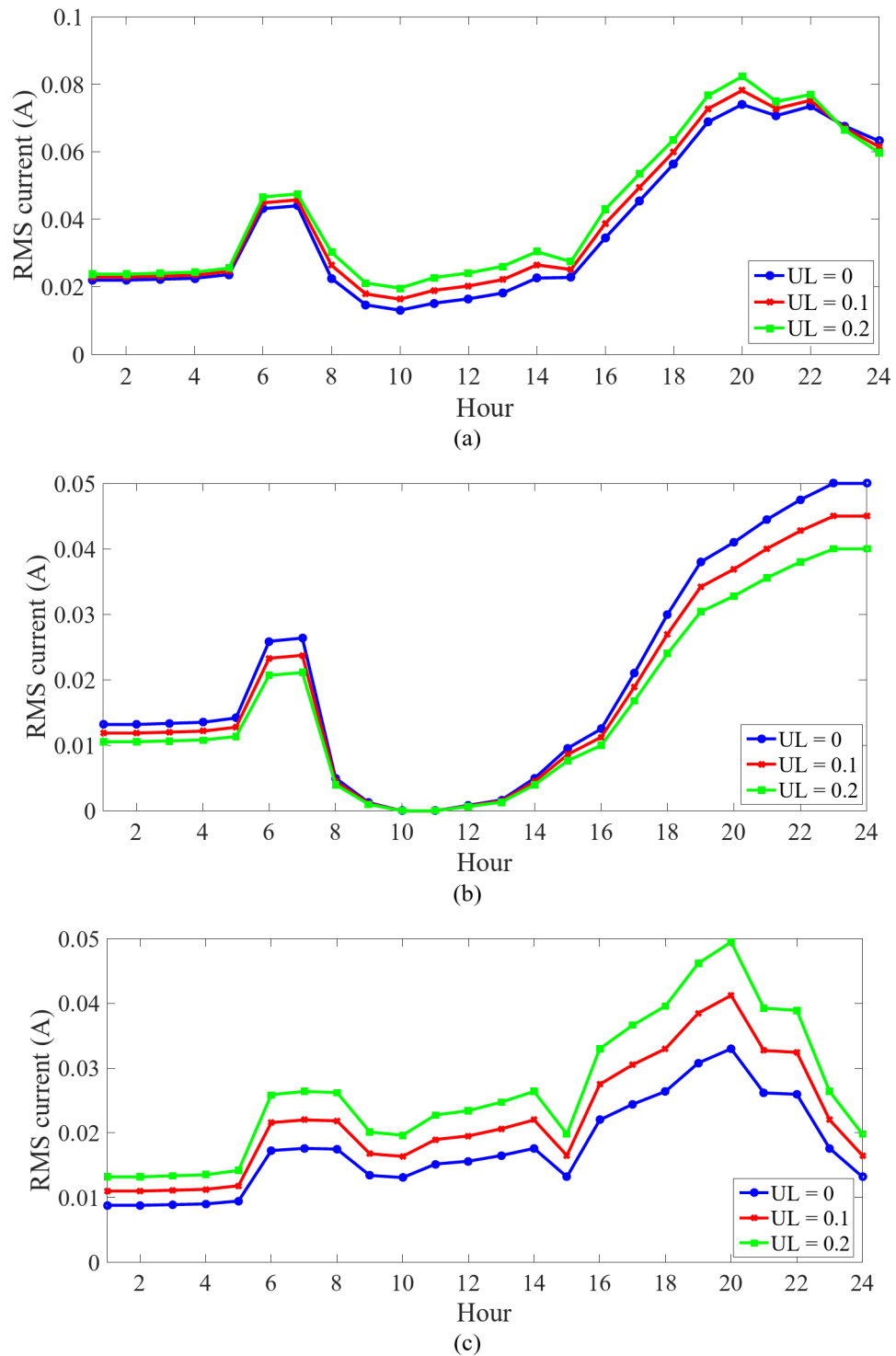


Fig. 8. Daily RMS harmonic current curve of, (a) FRIEsSs, (b) EVs, and (c) RESs for different value of UL in UB=1.

first case. In the field of the harmonic index, in which the maximum value of THD voltage is reported in this section, it is observed that its rate in the first case is about 7.83%. However, according to IEEE519 standard, the maximum allowable value of this index should be equal to 5%³⁰. To achieve this, only the RESs and EVs in the second and fourth cases were able to adjust the maximum THD voltage to less than 5%. In this regard, RESs have better capabilities than EVs, because according to Fig. 8(b) and 8(c), RESs are able to better address the harmonic currents from nonlinear loads than EVs. DRPs have no role in controlling the harmonic current, so the maximum voltage THD in the third case is 7.83%. Finally, compared to the first scenario, the suggested system in the fifth case with effective RES management and flexibility in the form of FRIEsS was able to enhance

UL	–	0	0.1	0.2	0	0.1	0.2
Case	I	II			III		
Energy loss (MWh)	1.937	1.412	1.540	1.672	1.722	1.808	1.889
Maximum voltage drop (p.u.)	0.092	0.047	0.048	0.049	0.061	0.063	0.064
Maximum over-voltage (p.u.)	0	0.014	0.013	0.012	0	0	0
Lower value of power factor in distribution station	0.815	0.906	0.903	0.901	0.893	0.889	0.885
Upper value of power factor in distribution station	0.815	1	1	1	0.951	0.947	0.944
Maximum voltage THD (%)	7.83	3.84	3.98	4.11	7.83	7.83	7.83
Case	I	IV			V		
Energy loss (MWh)	1.937	1.975	2.062	2.146	1.514	1.648	1.779
Maximum voltage drop (p.u.)	0.092	0.055	0.056	0.057	0.049	0.051	0.052
Maximum over-voltage (p.u.)	0	0	0	0	0.011	0.009	0.007
Lower value of power factor in distribution station	0.815	0.905	0.902	0.9	0.917	0.910	0.904
Upper value of power factor in distribution station	0.815	1	1	1	1	1	1
Maximum voltage THD (%)	7.83	4.02	4.13	4.23	3.53	3.67	3.82

Table 5. The rate of operation indicators and power quality (harmonic) for different levels of uncertainty in UB = 1.

all performance and harmonic indicators. So, in the worst-case situation, with UL=0.2 and UB=1, it was able to cut energy losses by about 8.2% $((1.779-1.937)/1.937)$ compared to the first instance. At UL=0, this rate is around 21.2%. At UL=0.2, with a maximum overvoltage of 0.007 per unit, it was able to lower the peak voltage reduction by approximately 43.5% when compared to the first scenario. It has also set the distribution power factor between 0.9 and 1. Finally, at UL=0.2 and UB=1, it was able to reduce the maximum THD voltage by about 51.2% compared to load distribution studies. On the other hand, by reducing the level of uncertainty to UL=0.2, the proposed scheme for the fifth has a higher ability to improve these indicators. Because in these conditions, according to Table (4), power and current consumption decrease with decreasing UL, and the ability of FRIESs to produce power and current increases. Therefore, according to the model framework outlined earlier chapter, FRIESs are able to play a more plays a significant role in enhancing the performance metrics and power quality than in the case UL=0. Over-voltage is created due to the integration of renewable energy sources into the network. Consequently, overvoltage exists only in cases II and V.

In this article, optimization is not performed on a predetermined scenario. In other words, in this article, the results are not presented only for the model that assumes deterministic conditions. In this article, robust optimization is used. Based on Sect. 3, robust optimization simultaneously obtains the most challenging conditions and the best achievable outcome under these conditions. The worst-case scenario presents values of uncertainties that have the worst value of the objective function in the worst-case scenario is compared to that in other scenarios. Also, different results have been obtained in Figs. 5, 6, 7 and 8; Tables 4 and 5 for different conditions of the robust model. In other words, by changing the setting parameters of the robust model, such as uncertainty budget (UB) and uncertainty level (UL), different states are obtained for the worst-case scenario, various scenarios arising from uncertainties are considered have been examined in the numerical results section.

Conclusion

The current work presents the best SDN power management with FRIESs by taking nonlinear load harmonic correction into account. RESs like WT and PV systems, as well as flexible resources like DRP and EV aggregation, are available in FRIES. Following the weighted sum of functions technique, the final model of the suggested design was developed as a three-objective optimization. The goal functions were to reduce the overall THD voltage, grid energy losses, and SDN operating costs. It is put via the RESs and flexibility as FRIES operation model and the AC-HOPF equations. The LP model was subsequently created from the NLP description of the concept. There are uncertainties in this with regard to load, energy costs, RESs, and EV energy use. Robust adaptive optimization is then used to represent these unknown quantities. Ultimately, the findings show that, while the NLP model solvers of the given design have diverse answers, the LP model solvers of the suggested model may produce a single optimum solution. Furthermore, the answer produced by LP solvers is superior than that of NLP solvers. Among the suggested LP problem solutions, the CPLEX solver has the lowest computing time. The suggested architecture is resistant to a maximum forecast error of 45% owing to uncertainties of demand, energy cost, RESs power and energy consumption of EVs and is able to obtain an optimum solution. The goal function is almost at its minimal value at the compromise point. As a result, SDN operating costs, grid energy losses, and overall voltage THD are about 17.7%, 18.8%, and 22.8% higher than their minimal points, respectively. In comparison to load flow studies in the scenario representing the most adverse conditions with an uncertainty level of 0.2, the proposed design with effective regulation of both active and reactive power and harmonic flow of resources as FRIES reduced grid energy losses, voltage profiles, and maximum THD voltage by about 8.2%, 43.5%, and 51.2%, respectively. Furthermore, the power factor ranged between 0.9 and 1. Of course, lowering the uncertainty level increases the percentage of improvement for the indices indicated.

In the proposed approach, the cost associated with operating the network has been evaluated. However, the implementation of the power and energy management requires equipment such as telecommunication devices,

smart algorithms and other items, which impose cost. Yet, this issue was not included in the proposed plan and it was considered as future work. In this article, it is assumed that the nonlinear loads have harmonic current. In addition, IES can create a harmonic current in the opposite direction of the harmonic current of the nonlinear load. Therefore, the level of harmonic current within the network reduces. According to the numerical findings, the voltage harmonics is not zero, so the current harmonic in the network is not zero. Therefore, resonance has not occurred in the network. But in general, no limit was considered for resonance in this article, but it was will be addressed as part of future research. The suggested approach, the electricity energy management is considered in IES. But, the different sources and storage can be controlled other energies such as heat energy. Hence, IES can be managed the different energies, where addressing this issue will be part of future research efforts.

Data availability

Data availability statement: The datasets used and/or analysed during the current study available from the corresponding author on reasonable request.

Received: 15 October 2024; Accepted: 7 February 2025

Published online: 24 February 2025

References

- Pirouzi, S., Latify, M. A. & Yousefi, G. R. Investigation on reactive power support capability of PEVs in distribution network operation. In: *23rd Iranian Conference on Electrical Engineering*, 1591–1596 (IEEE, 2015).
- Roustaeae, M. & Kazemi, A. Multi-objective energy management strategy of unbalanced multi-microgrids considering technical and economic situations. *Sustain. Energy Technol. Assess.* **47**, 101448 (2021).
- Aliabadi, M. J. & Radmehr, M. Hybrid energy system optimization integrated with battery storage in radial distribution networks considering reliability and a robust framework. *Sci. Rep.* **14**, 26597 (2024).
- Seyyedi, A. Z. G. et al. Bi-level siting and sizing of flexi-renewable virtual power plants in the active distribution networks. *Int. J. Electr. Power Energy Syst.* **137**, 107800 (2022).
- Roustaeae, M. & Kazemi, A. Multi-objective stochastic operation of multi-microgrids constrained to system reliability and clean energy based on energy management system. *Electr. Power Syst. Res.* **194**, 106970 (2021).
- Zhang, Y. et al. Optimizing the operation strategy of a combined cooling, heating and power system based on energy storage technology. *Sci. Rep.* **13**, 2928 (2023).
- Wu, C., Gu, W., Zhou, S. & Chen, X. Coordinated optimal power flow for integrated active distribution network and virtual power plants using decentralized algorithm. *IEEE Trans. Power Syst.* **36**, 3541–3551 (2021).
- Naughton, J., Wang, H., Cantoni, M. & Mancarella, P. Co-optimizing virtual power plant services under uncertainty: a robust scheduling and receding horizon dispatch approach. *IEEE Trans. Power Syst.* **36**, 3960–3972 (2021).
- Seyyedi, A. Z. G., Akbari, E., Rashid, S. M., Nejati, S. A. & Gitizadeh, M. Application of robust optimized spatiotemporal load management of data centers for renewable curtailment mitigation. *Renew. Sustain. Energy Rev.* **204**, 114793 (2024).
- Lou, N. et al. Two-stage congestion management considering virtual power plant with cascade hydro-photovoltaic-pumped storage hybrid generation. *IEEE Access.* **8**, 186335–186347 (2020).
- Yi, Z., Xu, Y., Zhou, J., Wu, W. & Sun, H. Bi-level programming for optimal operation of an active distribution network with multiple virtual power plants. *IEEE Trans. Sustain. Energy.* **11**, 2855–2869 (2020).
- Lee, J. & Won, D. Optimal operation strategy of virtual power plant considering real-time dispatch uncertainty of distributed energy resource aggregation. *IEEE Access.* **9**, 56965–56983 (2021).
- Vahedipour-Dahraie, M., Rashidizadeh-Kermani, H., Shafie-Khah, M. & Catalão, J. P. Risk-averse optimal energy and reserve scheduling for virtual power plants incorporating demand response programs. *IEEE Trans. Smart Grid.* **12**, 1405–1415 (2020).
- Foroughi, M., Pasban, A., Moeini-Aghaie, M. & Fayaz-Heidari, A. A bi-level model for optimal bidding of a multi-carrier technical virtual power plant in energy markets. *Int. J. Electr. Power Energy Syst.* **125**, 106397 (2021).
- Wang, Y., Gao, W., Qian, F. & Li, Y. Evaluation of economic benefits of virtual power plant between demand and plant sides based on cooperative game theory. *Energy. Conv. Manag.* **238**, 114180 (2021).
- Wang, L., Wu, W., Lu, Q. & Yang, Y. Optimal aggregation approach for virtual power plant considering network reconfiguration. *J. Mod. Power Syst. Clean. Energy.* **9**, 495–501 (2021).
- Dall'Anese, E., Guggilam, S. S., Simonetto, A., Chen, Y. C. & Dhople, S. V. Optimal regulation of virtual power plants. *IEEE Trans. Power Syst.* **33**, 1868–1881 (2017).
- Niaki, A. A. & Jamil, M. An efficient hydrogen-based water-power strategy to alleviate the number of transmission switching within smart grid. *Int. J. Hydrog. Energy.* **70**, 347–356 (2024).
- Seyyedi, A. Z. G. et al. Iterative optimization of a bi-level formulation to identify severe contingencies in power transmission systems. *Int. J. Electr. Power Energy Syst.* **145**, 108670 (2023).
- Bagchi, A., Goel, L. & Wang, P. Adequacy assessment of generating systems incorporating storage integrated virtual power plants. *IEEE Trans. Smart Grid.* **10**, 3440–3451 (2018).
- Fang, X., Dong, W., Wang, Y. & Yang, Q. Multi-stage and multi-timescale optimal energy management for hydrogen-based integrated energy systems. *Energy* **286**, 129576 (2024).
- Liang, H. & Pirouzi, S. Energy management system based on economic Flexi-reliable operation for the smart distribution network including integrated energy system of hydrogen storage and renewable sources. *Energy* **293**, 130745 (2024).
- Wang, L. L. et al. Cooperative operation of industrial/commercial/residential integrated energy system with hydrogen energy based on Nash bargaining theory. *Energy* **288**, 129868 (2024).
- Kiani, H., Hesami, K., Azarhooshang, A., Pirouzi, S. & Safaei, S. Adaptive robust operation of the active distribution network including renewable and flexible sources. *Sustainable Energy Grids Networks.* **26**, 100476 (2021).
- Mahmoudi Rashid, S., Rikhtehgar Ghiasi, A. & Ghaemi, S. A new distributed robust H_∞ control strategy for a class of uncertain interconnected large-scale time-delay systems subject to actuator saturation and disturbance. *J. Vib. Control* 10775463241259345. (2024).
- Dini, A., Pirouzi, S., Norouzi, M. & Lehtonen, M. Hybrid stochastic/robust scheduling of the grid-connected microgrid based on the linear coordinated power management strategy. *Sustainable Energy Grids Networks.* **24**, 100400 (2020).
- Rashid, S.M., Zare-Ghaleh-Seyyedi, A., Moosanezhad, J., Khan, A.A. Multi-objective design of the energy storage-based combined heat and power off-grid system to supply of thermal and electricity consumption energies. *J. Energy Storage.* **73**, 108675 (2023).
- Dall'Anese, E., Zhu, H. & Giannakis, G. B. Distributed optimal power flow for smart microgrids. *IEEE Trans. Smart Grid.* **4**, 1464–1475 (2013).
- Zeng, X. J., Zhai, H. F., Wang, M. X., Yang, M. & Wang, M. Q. A system optimization method for mitigating three-phase imbalance in distribution network. *Int. J. Electr. Power Energy Syst.* **113**, 618–633 (2019).

30. Gill, S., Kockar, I. & Ault, G. W. Dynamic optimal power flow for active distribution networks. *IEEE Trans. Power Syst.* **29**, 121–131 (2013).
31. Ma, Y. et al. Robust optimization model of flexible distribution network considering source-load uncertainty. *Electr. Power Syst. Res.* **223**, 109698 (2023).
32. Bertsimas, D., Litvinov, E., Sun, X. A., Zhao, J. & Zheng, T. Adaptive robust optimization for the security constrained unit commitment problem. *IEEE Trans. Power Syst.* **28**, 52–63 (2012).
33. Homayoun, R., Bahmani-Firouzi, B. & Niknam, T. Multi-objective operation of distributed generations and thermal blocks in microgrids based on energy management system. *IET Generation Trans. Dist.* **15**, 1451–1462. <https://doi.org/10.1049/gtd.12112> (2021).
34. Parsibenehkoal, R., Jamil, M. & Khan, A. A. A multi-stage framework for coordinated scheduling of networked microgrids in active distribution systems with hydrogen refueling and charging stations. *Int. J. Hydrog. Energy.* **71**, 1442–1455 (2024).
35. Jakob, W. & Blume, C. Pareto optimization or cascaded weighted sum: a comparison of concepts. *Algorithms* **7**, 166–185 (2014).
36. Herraiz, S., Sainz, L. & Clua, J. Review of harmonic load flow formulations. *IEEE Trans. Power Delivery.* **18**, 1079–1087 (2003).

Author contributions

Kai Jin: Conceptualization, Methodology, Software, Validation, Formal analysis, Investigation, Resources, Data Curation, Writing - Original Draft. Hamed Banizaman: Conceptualization, Software, Validation, Formal analysis, Investigation, Resources, Data Curation, Writing - Original Draft. Sina samadi gharehveran: Validation, Formal analysis, Investigation, Resources, Data Curation, Writing - Original Draft. Mohammad reza jokar: Conceptualization, Software, Investigation, Resources, Data Curation, Writing - Original Draft. Alireza Mohammadi Amidi: Conceptualization, Formal analysis, Investigation, Resources, Writing - Original Draft. Jianyong Yu: Conceptualization, Methodology, Curation, Writing - Original Draft. Hayder Olewi Shami: Software, Validation, Formal analysis, Investigation, Resources, Data Curation, Writing - Original Draft.

Declarations

Competing interests

The authors declare no competing interests.

Additional information

Correspondence and requests for materials should be addressed to H.B.

Reprints and permissions information is available at www.nature.com/reprints.

Publisher's note Springer Nature remains neutral with regard to jurisdictional claims in published maps and institutional affiliations.

Open Access This article is licensed under a Creative Commons Attribution-NonCommercial-NoDerivatives 4.0 International License, which permits any non-commercial use, sharing, distribution and reproduction in any medium or format, as long as you give appropriate credit to the original author(s) and the source, provide a link to the Creative Commons licence, and indicate if you modified the licensed material. You do not have permission under this licence to share adapted material derived from this article or parts of it. The images or other third party material in this article are included in the article's Creative Commons licence, unless indicated otherwise in a credit line to the material. If material is not included in the article's Creative Commons licence and your intended use is not permitted by statutory regulation or exceeds the permitted use, you will need to obtain permission directly from the copyright holder. To view a copy of this licence, visit <http://creativecommons.org/licenses/by-nc-nd/4.0/>.

© The Author(s) 2025